Intraseasonal Variability Associated with Asian Summer Monsoon Simulated by 14 IPCC AR4 Coupled GCMs

Jia-Lin Lin[1], Klaus M. Weickmann[1], George N. Kiladis[1], Brian E. Mapes[2], Siegfried D. Schubert[3], Max J. Suarez[3], Julio T. Bacmeister[3], and Myong-In Lee[3]

[1]NOAA ESRL/CIRES Climate Diagnostics Center, Boulder, CO
[2]RSMAS, University of Miami, Miami, FL
[3]NASA GSFC Global Modeling and Assimilation Office, Greenbelt, MD

Submitted to *J. Climate*
November 2006

Corresponding author address: Dr. Jia-Lin Lin
NOAA ESRL/CIRES Climate Diagnostics Center
325 Broadway, R/PSD1, Boulder, CO 80305-3328
Email: jialin.lin@noaa.gov

Abstract

This study evaluates the intraseasonal variability associated with the Asian summer monsoon in 14 coupled general circulation models (GCMs) participating in the Inter-governmental Panel on Climate Change (IPCC) Fourth Assessment Report (AR4). Eight years of daily precipitation from each model's 20th century climate simulation are analyzed and compared with daily satellite retrieved precipitation. We focus on the three major components of Asian summer monsoon: the Indian summer monsoon (ISM), the western North Pacific summer monsoon (WNPSM), and the east Asian summer monsoon (EASM), together with the two dominant intraseasonal modes: the eastward and northward propagating boreal summer intraseasonal oscillation (BSIO) and the westward propagating 12-24 day mode.

The results show that current state-of-the-art GCMs display a wide range of skill in simulating the intraseasonal variability associated with Asian summer monsoon. During boreal summer (May-October), most of the models produce reasonable seasonal mean precipitation over the ISM region, but excessive precipitation over WNPSM region and insufficient precipitation over EASM region. In other words, models concentrate their rain too close to the equator in the Western Pacific. Most of the models simulate overly weak total intraseasonal (2-128 day) variance, as well as too little variance for BSIO and the 12-24 day mode. Moreover, models often have difficulty in simulating the eastward propagation of BSIO. Nevertheless, many models simulate well the northward propagation of BSIO, together with the westward propagation of the 12-24 day mode. The northward propagation in these models is thus not simply a NW-SE tilted tail protruding off of an eastward-moving deep-tropical intraseasonal oscillation. Only 4-5

models produce spectral peaks in the BSIO and 12-24 day frequency bands; instead, most of the models display too red a spectrum, i.e. an overly strong persistence of precipitation.

1. Introduction

The Asian summer monsoon significantly affects the lives of more than 60% of the world's population. It has three major components (Figure 1): the Indian summer monsoon, the eastern Asian summer monsoon, and the western north Pacific summer monsoon (see review by Wang and Linho 2002). It also has strong intraseasonal variability with two dominant modes: an eastward- and northward-propagating boreal summer intraseasonal oscillation (BSIO) with a period of about 24-70 days (e.g. Yasunari 1979; Murakami and Nakazawa 1985; Lau and Chan 1986; Knutson et al. 1986; Wang and Rui 1990; Kemball-Cook and Wang 2001; Hsu and Weng 2001; Lawrence and Webster 2002; Straub and Kiladis 2003; Jiang et al. 2004; among many others), and a westward-propagating mode with a period of about 12-24 days (hereafter referred to as the 12-24 day mode; e.g. Krishnamurti and Ardanuy 1980; Murakami 1980; Lau et al. 1988; Lau and Lau 1990; Hartmann et al. 1992; Chen and Chen 1993, 1995; Kiladis and Weickmann 1997; Vincent et al. 1998; Fukutomi and Yasunari 1999, 2002; Chen et al. 2000). These intraseasonal modes significantly affect the onset and breaks of all the three monsoon regions, and the formation, intensity and track of the tropical cyclones (e.g. Liebmann et al. 1994). Therefore, they are important for both weather prediction and climate prediction.

Unfortunately, the intraseasonal variability of Asian summer monsoon has not been well simulated in general circulation models (GCMs) used for weather predictions, climate predictions, and climate projections (e.g. Sperber et al. 2001; Wu et al. 2002; Waliser et al. 2003a, b, c). For example, in an evaluation of the simulations of 10 Atmospheric GCMs, Waliser et al. (2003c) found that the model BSIO patterns are

typically less coherent, lack sufficient eastward propagation, and have smaller zonal and meridional spatial scales than the observed patterns, and are often limited to one side or the other of the maritime continent. The most pervasive and problematic feature of the models' depiction of intraseasonal variability and/or their BSIO patterns is the overall lack of variability in the equatorial Indian Ocean. These biases are detrimental to both weather prediction and climate prediction.

Factors that are possibly important for BSIO simulations include model physics, model resolution, and air-sea coupling. Most of the previous GCM sensitivity studies of BSIO simulation focused on the role of air-sea coupling, and found that air-sea coupling significantly improves the BSIO signals (e.g. Kemball-Cook et al. 2002; Fu et al. 2003; Fu and Wang 2004a,b). However, changes in a model's mean state need to be taken into account (e.g. Kemball-Cook et al. 2002), which strongly affects wave-heating feedback in BSIO, for example, by providing the mean surface wind that determines the sign of WISHE (Wind Induced Surface Heat Exchange) feedback (Emanuel 1987, Neelin et al. 1987), or by providing strong equivalent linear mechanical damping making the BSIO a highly viscous oscillation (Lin et al. 2005).

Recently, in preparation for the Inter-governmental Panel on Climate Change (IPCC) Fourth Assessment Report (AR4), more than a dozen international climate modeling centers conducted a comprehensive set of long-term simulations for both the 20th century's climate and different climate change scenarios in the 21st century. Before conducting the extended simulations, many of the modeling centers applied an overhaul to their physical schemes to incorporate the state-of-the-art research results. For example, almost all modeling centers have implemented prognostic cloud microphysics schemes to

their models, some have added a moisture trigger to their deep convection schemes, and some now take into account convective momentum transport. Moreover, many modeling centers increased their models' horizontal and vertical resolutions and some conducted experiments with different resolutions. Some also did AMIP runs in addition to the standard coupled runs. Therefore, it is of interest to assess the MJO simulations in this new generation of climate models to look at the effects of the updated physical processes, higher resolution and air-sea coupling. Such an evaluation is also important for evaluating the general performance of the climate models used for climate change projections in the IPCC AR4.

Lin et al. (2006) evaluated the MJO and convectively coupled equatorial waves in 14 IPCC AR4 models. The results show that current state-of-the-art GCMs still have significant problems and display a wide range of skill in simulating tropical intraseasonal variability. The total intraseasonal (2-128 day) variance of precipitation is too weak in most of the models. About half of the models have signals of convectively coupled equatorial waves, but the variances are generally too weak and the phase speeds are generally too fast, suggesting that the models may not have a large enough reduction in their "effective static stability" by diabatic heating. Most of the models produce overly weak MJO variance and poor MJO propagation. Moreover, the MJO variance in 13 of the 14 models does not come from a pronounced spectral peak, but usually comes from part of an over-reddened spectrum, which in turn is associated with too strong persistence of equatorial precipitation. The two models that arguably do best at simulating the MJO are the only models having convective closures/triggers linked in some way to moisture convergence.

The purpose of this study is to extend the Lin et al. (2006) analysis to evaluate the intraseasonal variability associated with Asian summer monsoon in IPCC AR4 coupled GCMs, with an emphasis on the BSIO and 12-24 day mode. All the previous model intercomparison studies used Atmospheric GCMs forced by observed SSTs (e.g. Sperber et al. 2001; Wu et al. 2002; Waliser et al. 2003a, b, c), and the present study, to our knowledge, is the first coupled GCM intercomparison in the literature for Asian summer monsoon intraseasonal variability. If air-sea coupling does indeed significantly improve GCM's simulations of Asian summer monsoon intraseasonal variability (e.g. Kemball-Cook et al. 2002; Fu and Wang 2004a,b), the coupled models should be expected to perform better. The questions we address are:

(1) How well do the IPCC AR4 models simulate the intraseasonal precipitation signals associated with Asian summer monsoon, especially the BSIO?

(2) Is there any systematic dependence of model BSIO simulations on the basic characteristics of convection schemes, such as closure assumption, or model resolution?

(3) Is there any connection between the models' BSIO simulations and their MJO simulations?

(4) Do coupled models do better than uncoupled models?

The models and validation datasets used in this study are described in section 2. The diagnostic methods are described in section 3. Results are presented in section 4. A summary and discussion are given in section 5.

2. Models and validation datasets

This analysis is based on eight years of the Climate of the 20th Century (20C3M) simulations from 14 coupled GCMs. Table 1 shows the model names and acronyms, their horizontal and vertical resolutions, and brief descriptions of their deep convection schemes. For each model we use eight years of daily mean surface precipitation.

The model simulations are validated using the Global Precipitation Climatology Project (GPCP) Version 2 Precipitation (Huffman et al. 2001). We use eight years (1997-2004) of daily data with a horizontal resolution of 1 degree longitude by 1 degree latitude.

3. Method

BSIO variability can be decomposed into two components: an eastward propagating component and a northward propagating component. The eastward component is defined as rainfall variability in eastward zonal wavenumbers 1-6 and in the period range of 24-70 days, while the northward component is defined as northward propagating 24-70 day variability which includes all meridional wavenumbers. As shown by previous observational studies (e.g. Fu et al. 2003), the northward component of BSIO is dominated by the largest meridional wavenumber within the latitude range of the analysis (5-25N). Therefore, although we include all meridional wavenumbers, the isolated signal is dominated by the largest wavenumber, as will be shown later in section 4c.

The eastward component of BSIO is isolated using the following procedure: (1) The 8 years of daily precipitation data was averaged along the latitude belt between 5N and 25N, where the eastward propagation of BSIO mainly happens, with a zonal resolution of

10 degrees longitude. (2) The space-time spectrum was calculated using discrete Fourier transform for the whole 8-year time series. (3) Then we used an inverse space-time Fourier transform to get the time series of the eastward wavenumbers 1-6 component, which includes all available frequencies. (4) Then these time series were filtered using a 365-point 24-70 day Lanczos filter (Duchan 1979). Because the Lanczos filter is non-recursive, 182 days of data were lost at each end of the time series (364 days in total). (5) The resultant eastward wavenumbers 1 through 6, 24-70 day anomaly during northern summer (May-October) is hereafter referred to as the eastward component of the BSIO anomaly. (6) Its variance was also compared with the variance of its westward counterpart, i.e., the westward wavenumbers 1-6, 24-70 day anomaly, which was isolated using the same method as above.

The northward component of BSIO was isolated using the same procedure as above except for the northward 24-70 day mode including all meridional wavenumbers, which is similar to the procedure in Fu and Wang (2004a, b). The space-time Fourier analysis was applied to the latitude range between 45S and 45N. Although precipitation is very small at 45S and 45N, we still tap the data to zero at each end to get a strict periodicity for this meridional section. The variance of the northward component of BSIO was averaged over two longitude belts: 70E-100E (the ISM region) and 120E-160E (the WNPSM and EASM regions). It was also compared with the variance of its southward counterpart, i.e., the southward 24-70 day anomaly, which was isolated using the same method as above.

The procedure for isolating the 12-24 day mode is also same as above except for the westward 12-24 day mode including all zonal wavenumbers. Its variance was also

compared with the variance of its eastward counterpart, i.e., the eastward 12-24 day anomaly, which was isolated using the same method as above.

4. Results

a Boreal summer (May-October) seasonal mean precipitation and seasonal variation

Previous observational studies indicate that the intraseasonal variance of convection is highly correlated with time-mean convective intensity (e.g. Wheeler and Kiladis 1999, Hendon et al. 1999). Therefore we first look at the boreal summer (May-October) seasonal mean precipitation in the three Asian summer monsoon regions: the ISM region, the EASM region, and the WNPSM region (Fig. 1). Figure 2a shows the zonal profile along the latitude belt averaged between 5N and 25N. Most of the models produce reasonable seasonal mean precipitation in the ISM region (60E-100E), but overly large precipitation in the WNPSM region (110E-170E), which is associated with an overall overestimate of precipitation along the Pacific ITCZ. Figure 2b shows the zonal profile averaged between 25N and 40N. All models invariably underestimate the seasonal mean precipitation in the EASM region (100E-160E).

To look at the detailed meridional distribution, we plot in Figure 3a the meridional profile averaged between 60E and 100E (the ISM region). In observation the maximum precipitation in the northern hemisphere lies between 12N and 22N, but in many models the maximum lies closer to the equator around 12N. The reasonable area-mean precipitation for the ISM region in many models (Figure 2a) actually comes from compensation between excessive precipitation close to the equator and insufficient precipitation far from the equator. This problem is even more prominent in the meridional

profile averaged between 100E and 160E (Figure 3b), leading to the excessive precipitation over WNPSM region (5N-25N) but insufficient precipitation over EASM region (25N-40N).

Figure 4 shows the seasonal cycle of precipitation averaged over the three monsoon regions. For the ISM region (Figure 4a), most of the models reproduce the monsoon onset in May. However, many models tend to produce excessive precipitation from July to September (e.g. MIROC-medres, MIROC-hires, CNRM, CCSM3, CGCM). For the WNPSM region (Figure 4b), most of the models simulate well the phase of seasonal cycle, but produce excessive precipitation throughout the whole seasonal cycle. For the EASM region (Figure 4c), most of the models do not have significant seasonal variation, with insufficient precipitation during summer but excessive precipitation during winter.

In summary, most of the IPCC AR4 climate models produce reasonable seasonal mean precipitation over the ISM region, but excessive precipitation over WNPSM region and insufficient precipitation over EASM region. Models tend to produce excessive precipitation close to the equator but insufficient precipitation far from the equator. Most of the models reproduce well the phase of seasonal cycle in the ISM and WNPSM region, but produce too-weak seasonal variation in the EASM region.

b Total intraseasonal (2-128 day) variance

Figure 5a shows the meridional profile of total intraseasonal (2-128 day) variance of precipitation in the ISM region averaged between 60E-100E. The total intraseasonal variance in most of the models is smaller than in observation. The variance in three models (ECHAM5/MPI-OM, MIROC3.2-medres and MIROC3.2-hires) approaches the

observed value in the ISM region (5N-25N), although it is too small on the equator in the later two models.

Figure 5b shows the total intraseasonal variance in the WNPSM and EASM regions. Again, most of the models produce overly small variances in both regions. Only one model (ECHAM5/MPI-OM) produces realistic variance in the WNPSM region (5N-25N), and one model (MIROC3.2-hires) produces relatively large variance in the EASM region (25N-40N).

In summary, the total intraseasonal (2-128 day) variance of precipitation in most models is smaller than in observations. Only a couple of models simulate realistic variance in one or two of the monsoon regions, but no model can reproduce the observed values in all the three monsoon regions.

c The eastward component of BSIO

Now we focus on the variance of the eastward component of BSIO (hereafter BSIO-E), i.e., the daily variance of the eastward wavenumbers 1-6, 24-70 day mode. Figure 6 shows the variance of BSIO-E along the equator averaged between 5N and 25N. In observation the BSIO-E variance has its maximum over the Indian Ocean, but many models produce the largest variance over maritime continent or western Pacific, which may be associated with the excessive seasonal-mean precipitation over the WNPSM region in many models (Figure 2a). The model variance approaches the observed value in three of the 14 models over the WNPSM region (ECHAM5/MPI-OM, CNRM, and CGCM), but is less than half of the observed value in all other 11 models. This is similar to the performance of the IPCC AR4 models in simulating the MJO, for which the simulated variance is less than half of the observed value in 12 of the 14 models.

In addition to the variance, another important index for evaluating the BSIO-E simulation is the ratio between the variance of the eastward BSIO-E and that of its westward counterpart, i.e., the westward wavenumbers 1-6, 24-70 day mode, which is for a measure of the zonal propagation of tropical intraseasonal oscillation. Figure 7 shows the ratio between the eastward variance and the westward variance averaged over an Indian Ocean box between 5N-25N and 70E-130E. In observation, the eastward BSIO-E variance is about 1.5 times of the westward variance. Of the 14 models, four models simulate a realistic or too-large ratio (GFDL2.0, PCM, CGCM, and CSIRO), but all other 10 models produce a too-small ratio that is nearly equal to one, or even less than one (i.e., westward variance dominates over eastward variance).

The competition between the eastward MJO variance and its westward counterpart largely determines the zonal propagation characteristics of tropical intraseasonal oscillation. A useful method for evaluating the MJO simulation is to look at the propagation of 30-70 day filtered anomaly of the raw precipitation data, which includes all wavenumbers, to see if the BSIO-E mode (the eastward wavenumbers 1-6 mode) dominates over other modes, as is the case in observations. Figure 8 shows the lag-correlation of 30-70 day precipitation anomaly averaged between 5N and 25N with respect to itself at 95E. The observational data shows prominent eastward propagating signals of the BSIO-E, with a phase speed of about 5 m/s. The models display a wide range of propagation characteristics that are consistent with the ratio between the eastward BSIO-E variance and its westward counter part shown in Figure 7. The four models with a realistic or too large ratio (GFDL2.0, PCM, CGCM, and CSIRO) show a highly coherent eastward propagating signal. The phase speed is realistic in GFDL2.0,

but is too slow in PCM, CGCM, and CSIRO. Other models with the eastward/westward ratio nearly equal to one or less than one show a standing oscillation (e.g. GFDL2.1, GISS-AOM) or westward propagation (e.g. MIROC-medres, MIROC-hires).

To summarize, the model BSIO-E variance approaches the observed value over maritime continent/western Pacific in three of the 14 models, but is less than half of the observed value in the other 11 models. The ratio between the eastward BSIO-E variance and its westward counterpart is too small in most of the models, which is consistent with the lack of highly coherent eastward propagation of the BSIO in many models.

d The northward component of BSIO

Next we look at the variance of the northward component of BSIO (hereafter BSIO-N), i.e., the daily variance of the northward 24-70 day mode. Figure 9 shows the variance of the BSIO-N anomaly averaged between (a) 70E-100E (the ISM region), and (b) 120E-160E (the WNPSM/EASM region). For both regions, the BSIO-N variance is less than half of the observed value in nine models. There is no one-to-one correspondence between the models with large BSIO-N variance (more than half the observed) and those with large BSIO-E variance (Figure 6). Two models do simulate large variance for both BSIO-E and BSIO-N (MPI and CNRM), but some only simulate large BSIO-N variance (GFDL2.0, GFDL2.1, MIROC-medres), and one model only simulate large BSIO-E variance (CGCM).

Figure 10 shows the ratio between the northward BSIO-N variance and the variance of its southward counterpart averaged over (a) an ISM box between 5N-20N and 70E-100E, and (b) a WNPSM box between 5N-20N and 120E-160E. Over the ISM region (Figure 10a), the northward BSIO-N variance roughly quadruples the southward variance

in observation. Most of the models simulate a large ratio that is larger than two, although only one model (CNRM) produces a ratio that is larger than the observed value. This is in sharp contrast with the models' inability to simulate a large eastward/westward ratio for BSIO-E. Over the WNPSM region (Figure 10b), again, the northward BSIO-N variance nearly triples its southward counterpart in observation, and most of the models do produce a large ratio that is larger than 1.5.

Again following the analysis used for E-W propagation, the competition between the northward BSIO-N variance and its southward counterpart largely determines the meridional propagation characteristics of intraseasonal precipitation anomalies. Figure 11 shows the lag-correlation of 24-70 day precipitation anomaly averaged between 70E and 100E with respect to itself at 85E. The observational data shows prominent northward propagating signals of the BSIO-N, with a phase speed of about 1.8 m/s. Most of the models display a highly coherent northward propagating signal that is consistent with the large ratio between the northward BSIO-N variance and its southward counter part shown in Figure 10a. The only model with the ratio being nearly equal to one (GISS-AOM) shows a standing oscillation. The results are similar for the WNPSM region (not shown).

To summarize, the BSIO-N variance is too small in all models, and less than half of the observed value in the nine models. There is no one-to-one correspondence between the models with large BSIO-N variance and those with large BSIO-E variance, although two models (MPI and CNRM) do simulate large variance for both BSIO-E and BSIO-N. The ratio between the northward BSIO-N variance and the variance of its southward counterpart is too small but still at least half of the observed value in most of the models,

consistent with the highly coherent northward propagation of the BSIO-N in many models.

e The 12-24 day mode

Figure 12 shows the variance of the westward 12-24 day mode averaged between 10N-20N. Two of the 14 models (MPI and MRI) simulate overly large variance of the 12-24 day mode, and five other models (CNRM, CSIRO, GFDL2.1, MIROC-medres, and MIROC-hires) produce variance that is more than half of the observed value. However, the observed variance has its maximum over western Pacific but in some of the models the maximum is over the Indian Ocean (e.g. MIROC-medres and MIROC-hires).

Figure 13 shows the ratio between the variance of the westward 12-24 day mode and that of its eastward counterpart averaged over a western Pacific box between 10N-20N and 120E-170E. In observation, the westward variance is roughly double the eastward variance. All models simulate a ratio larger than one (i.e., westward variance dominates over eastward variance), and more than half of the models simulate an overly large ratio. As a result, most of the models display a highly coherent westward propagation of the 12-24 day mode (not shown).

In summary, the variance of the 12-24 day mode is typically too small, but rises to at least half of the observed value in half of the 14 models, and is even overly large in two models. Highly coherent westward propagation of the 12-24 day mode is seen in most of the models.

f Spectrum and auto-correlation of precipitation

Next we apply more detailed scrutiny to the intraseasonal variability of Asian monsoon precipitation by looking at the shape of the temporal power spectrum. Figure 14a shows the spectra at 15N115E (within the WNPSM region). The observational data shows prominent spectral peaks in both the 24-70 day frequency band, which correspond to BSIO, and the 12-24 day frequency band, which correspond to the 12-24 day mode. Only 4-5 models produce spectral peaks in both frequency bands (e.g. MIROC-medres, MPI, CNRM, and GFDL2.0), but most of them show too large variance at periods longer than 70 days, i.e., the spectrum is too red. Most of the other models without prominent spectral peak also display a too-red spectrum. The model spectra at 32N115E (within the EASM region) are even worse than at 15N115E. Most of the models fail to produce the spectral peaks for either the BSIO or the 12-24 day mode, but display a too-red spectrum.

The redness of many model spectra shown in Figure 14 brings to mind a "red noise" spectrum of a first-order linear Markov process (Gilman 1963; Jenkins and Watts 1968; Lin et al. 2006). For the first-order Markov process, the redness of the spectrum is determined by its lag-one auto-correlation ρ, hereafter referred to as the persistence of the time series. Therefore we plot in Figure 15 the auto-correlation function of precipitation at 15N115E. The observational data has a ρ of about 0.8. Most of the models have too large values of ρ, which are consistent with their spectra being too red (Figure 14a). Several models (e.g. CNRM and MIROC-medres) have a ρ similar to the observed value, which is consistent with the existence of prominent peaks in their spectra, i.e. with reduced power at the low frequency end of the intraseasonal range.

In short, 4-5 models produce spectral peaks for the BSIO and 12-24 day mode, while most of the models display too red a spectrum, which is consistent with the overly strong persistence of precipitation in those models.

5. Summary and discussion

The results above show that current state-of-the-art GCMs display a wide range of skill in simulating the intraseasonal variability associated with Asian summer monsoon. During boreal summer (May-October), most of the models produce reasonable seasonal mean precipitation over the ISM region, but excessive precipitation over WNPSM region and insufficient precipitation over EASM region. In other words, models concentrate their rain too close to the equator in the Western Pacific. Whether this indicates too little extratropical synoptic forcing, or too little response of precipitation to that forcing, is unclear. Most of the models simulate overly weak total intraseasonal (2-128 day) variance, as well as too little variance for BSIO and the 12-24 day mode. Moreover, models often have difficulty in simulating the eastward propagation of BSIO. Nevertheless, many models simulate well the northward propagation of BSIO, together with the westward propagation of the 12-24 day mode. Only 4-5 models produce spectral peaks in the BSIO and 12-24 day frequency bands; instead, most of the models display too red a spectrum, i.e. an overly strong persistence of precipitation.

As discussed in the introduction, factors hypothesized to be important for simulating boreal summer intraseasonal variability include air-sea coupling, model resolution, and model physics. Regarding air-sea coupling, all the models analyzed in this study are coupled GCMs, but they still have significant difficulties in simulating the intraseasonal

variability. As Hendon (2000) stated, coupling is "no panacea" for intraseasonal simulations. Still, it could be argued that coupling is important but hinges on the model details, background state. Without detailed experimentation using coupled and uncoupled versions of the same model, few firm conclusions can be drawn. Regarding model resolution, we have only one pair of similar atmospheric models but with different resolution: MIROC-hires (T106) vs MIROC-medres (T42). Higher model resolution does not increase the variances of either BSIO (Figure 6) or 12-24 day mode (Figure 12), although it slightly improves the westward propagation of the 12-24 day mode (Figure 13).

Regarding model physics, our results may suggest a few speculations. First, although there is no one-to-one correspondence between the models with large BSIO-E variance (Figure 6) and those with large BSIO-N variance (Figure 9), two models do simulate large variance for both BSIO-E and BSIO-N (MPI and CNRM), and *they are the only models with convective closure/trigger linked to moisture convergence*. As shown by Lin et al. (2006), these two models also do the best in simulating the boreal winter MJO. In contrast, in a set of 1990s era AMIP models, Slingo et al. (1996) found that deep convection schemes with CAPE-type closure tend to produce more realistic MJO signals than schemes with moisture-convergence-type closures. This peculiar reversal may just be a coincidence among a sample of just a handful of models, although perhaps we can at least conclude that convective closures/triggers may be a key aspect of model physics, in determining how convection feeds back on large-scale transient circulations like the MJO and BSIO.

Second, an overly red spectrum of precipitation is seen in many models (overly strong persistence of equatorial precipitation). As discussed in Lin et al. (2006), the persistence of equatorial precipitation may be amenable to improvement via changes in moist physics, for example by including self-suppression processes in tropical deep convection such as moisture triggers (i.e. dryness cutoffs), and the effects of convective and mesoscale downdrafts. Ultimately, such notions must be tested with careful experimentation in a controlled setting (a single model), but we hope that model intercomparion exercises like this may serve as useful input for hypothesis generation.

An interesting result of this study is that many models simulate well the northward propagation of BSIO. Previous theoretical and observational studies have suggested several mechanisms for the northward propagation of BSIO, including land surface heat flux (Webster 1983; Srinivasan et al. 1993), Rossby wave emanation (Wang and Xie 1996), vertical-shear-induced boundary layer moisture convergence (Jiang et al. 2004), moisture advection (Jiang et al. 2004), and ocean surface sensible heat flux (Hsu et al. 2004). Since in both observation and many IPCC AR4 models the strongest northward propagating signals appear over the northern Indian Ocean or western Pacific Ocean (Figure 9), the land surface heat flux may not play a significant role. Since many models producing good northward propagating signals fail to produce eastward propagating signals, the northward propagation is thus evidently not simply a NW-SE tilted tail protruding off of an eastward-moving deep-tropical intraseasonal oscillation, at least in these models. In future studies, analyses of heat, moisture and vorticity budgets are needed to examine if other mechanisms mentioned above contribute to the northward signals in the models.

In summary, we still have a long way to go to understand and overcome GCMs' difficulty in simulating intraseasonal variability associated with Asian summer monsoon. The importance of BSIO and 12-24 day variability for potential subseasonal (week two or week three) prediction of monsoon variability strongly warrant an unrelenting commitment to research in this direction.

Acknowledgements

Gary Russell kindly provided detailed description of the GISS-AOM model. We acknowledge the international modeling groups for providing their data for analysis, the Program for Climate Model Diagnosis and Intercomparison (PCMDI) for collecting and archiving the model data, the JSC/CLIVAR Working Group on Coupled Modeling (WGCM) and their Coupled Model Intercomparison Project (CMIP) and Climate Simulation Panel for organizing the model data analysis activity, and the IPCC WG1 TSU for technical support. The IPCC Data Archive at Lawrence Livermore National Laboratory is supported by the Office of Science, U.S. Department of Energy. J. L. Lin was supported by the U.S. CLIVAR CMEP Project, NOAA CPO/CVP Program, and NASA MAP Program. B. E. Mapes was supported by NSF ATM-0336790K and NOAA OGP CLIVAR-Pacific Program. George Kiladis was supported by NOAA CPO under grant GC05-156.

REFERENCES

Adler, R.F., G.J. Huffman, A. Chang, R. Ferraro, P. Xie, J. Janowiak, B. Rudolf, U. Schneider, S. Curtis, D. Bolvin, A. Gruber, J. Susskind, and P. Arkin, 2003: The Version 2 Global Precipitation Climatology Project (GPCP) Monthly Precipitation Analysis (1979-Present). J. Hydrometeor., 4,1147-1167.

Bougeault, P., 1985: A Simple Parameterization of the Large-Scale Effects of Cumulus Convection. *Monthly Weather Review*, 113, 2108–2121.

Chen, T.-C., and J.-M. Chen, 1993: The 10–20-Day Mode of the 1979 Indian Monsoon: Its Relation with the Time Variation of Monsoon Rainfall. Mon. Wea. Rev., 121, 2465-2482.

Chen, T.-C., and J.-M. Chen, 1995: An Observational Study of the South China Sea Monsoon during the 1979 Summer: Onset and Life Cycle. Mon. Wea. Rev., 123, 2295-2318.

Chen, T.-C., M.-C. Yen, and S.-P. Weng, 2000: Interaction between the Summer Monsoons in East Asia and the South China Sea: Intraseasonal Monsoon Modes. J. Atmos. Sci., 57, 1373-1392.

Del Genio, A. D., and M.-S. Yao, 1993: Efficient cumulus parameterization for long-term climate studies: The GISS scheme. *The Representation of Cumulus Convection in Numerical Models, Meteor. Monogr.,* No. 46, Amer. Meteor. Soc., 181–184.

Duchan, C.E., 1979: Lanczos filtering in one and two dimensions. *J. Appl. Meteor.*, **18**, 1016-1022.

Emanuel, K. A., 1987: An Air-Sea Interaction Model of Intraseasonal Oscillations in the Tropics. J. Atmos. Sci., 44, 2324-2340.

Emanuel, K. A., 1991: A Scheme for Representing Cumulus Convection in Large-Scale Models. *J. Atmos. Sci.*, 48, 2313–2329.

Emori, S., T. Nozawa, A. Numaguti and I. Uno (2001): Importance of cumulus parameterization for precipitation simulation over East Asia in June, J. Meteorol. Soc. Japan, 79, 939-947.

Fu, X., B. Wang, T. Li, and J. P. McCreary, 2003: Coupling between northward-propagating, intraseasonal oscillation and sea surface temperature in the Indian Ocean. J. Atmos. Sci., 60, 1733-1753.

Fu, X., and B. Wang, 2004a: Differences of Boreal Summer Intraseasonal Oscillations Simulated in an Atmosphere–Ocean Coupled Model and an Atmosphere-Only Model. J. Climate, 17, 1263-1271.

Fu, X., and B. Wang, 2004b: The Boreal-Summer Intraseasonal Oscillations Simulated in a Hybrid Coupled Atmosphere–Ocean Model. Mon. Wea. Rev., 132, 2628-2649.

Fukutomi, Y., and T. Yasunari, 1999: 10-25 day intraseasonal variation of convection and circulation over East Asia and western North Pacific during early summer. J. Meteor. Soc. Japan, 77, 753-769.

Fukutomi, Y., and T. Yasunari, 2002: Tropical-extratropical interaction associated with the 10-25 day oscillation over the western Pacific during the northern summer. J. Meteor. Soc. Japan, 80, 311-331.

Hartmann, D. L., M. L. Michelsen, and S. A. Klein, 1992: Seasonal variations of tropical intraseasonal oscillations: A 20–25 day oscillation in the western Pacific. J. Atmos. Sci., 49, 1277–1289.

Hsu H.-H., and C.-H. Weng, 2001: Northwestward propagation of the intraseasonal oscillation in the western North Pacific during the boreal summer: Structure and mechanism. *J. Climate*, **14**, 3834–3850.

Hsu H.-H., C.-H. Weng, and C.-H. Wu, 2004: Contrasting Characteristics between the Northward and Eastward Propagation of the Intraseasonal Oscillation during the Boreal Summer. *J. Climate*, 17, 727-743.

Huffman, G.J., R.F. Adler, M.M. Morrissey, S. Curtis, R. Joyce, B. McGavock, and J. Susskind, 2001: Global precipitation at one-degree daily resolution from multi-satellite observations. *J. Hydrometeor.*, **2**, 36-50.

Jiang, X., T. Li, and B. Wang, 2004: Structures and Mechanisms of the Northward Propagating Boreal Summer Intraseasonal Oscillation. J. Climate, 17, 1022-1039.

Kemball-Cook, S., and B. Wang. 2001: Equatorial Waves and Air–Sea Interaction in the Boreal Summer Intraseasonal Oscillation. *Journal of Climate*, 14, 2923–2942.

Kemball-Cook, S., B. Wang, and X. Fu, 2002: Simulation of the Intraseasonal Oscillation in the ECHAM-4 Model: The Impact of Coupling with an Ocean Model. J. Atmos. Sci., 59, 1433-1453.

Kiladis, G. N., and K. M. Weickmann, 1997: Horizontal Structure and Seasonality of Large-Scale Circulations Associated with Submonthly Tropical Convection. Mon. Wea. Rev., 125, 1997-2013.

Krishnamurti, T. N., and P. Ardanuy, 1980: The 10- to 20- day westward propagating mode and “breaks in the monsoon”. Tellus, 33, 15-26.

Krishnan R., and C. Venkatesan, 1997: Mechanisms of low frequency intraseasonal oscillation of the Indian summer monsoon. *Meteor. Atmos. Phys.*, **62**, 101–128.

Knutson, T. R., and K. M. Weickmann, 1987: 30–60 Day Atmospheric Oscillations: Composite Life Cycles of Convection and Circulation Anomalies. *Monthly Weather Review*, 115, 1407–1436.

Knutson, T. R., Klaus M. Weickmann and John E. Kutzbach. 1986: Global-Scale Intraseasonal Oscillations of Outgoing Longwave Radiation and 250 mb Zonal Wind during Northern Hemisphere Summer. *Monthly Weather Review*, 114, 605–623.

Lau, K. M., G.J. Yang, and S.H. Shen, 1988: Seasonal and Intraseasonal Climatology of Summer Monsoon Rainfall over Eeat Asia. Mon. Wea. Rev., 116, 18-37.

Lau, W. K. M., and D. E. Waliser, Eds., *"Intraseasonal Variability of the Atmosphere-Ocean Climate System"*, Springer, Heidelberg, Germany, 474pp.

Lau, K.-H., and N.-C. Lau, 1990: Observed Structure and Propagation Characteristics of Tropical Summertime Synoptic Scale Disturbances. Mon. Wea. Rev., 118, 1888-1913.

Lawrence, D. M., and P. J. Webster. 2002: The Boreal Summer Intraseasonal Oscillation: Relationship between Northward and Eastward Movement of Convection. *Journal of the Atmospheric Sciences*, 59, 1593–1606.

Lee, M.-I., I.-S. Kang, and B.E. Mapes, 2003: Impacts of cumulus convection parameterization on aqua-planet AGCM simulations of tropical intraseasonal variability. *J. Meteor. Soc. Japan,* **81**, 963-992.

Lin, J. L., 2006: The double-ITCZ problem in IPCC AR4 coupled GCMs: Ocean-atmosphere feedback analysis. *J. Climate*, accepted with minor revisions.

Lin, J. L., and B. E. Mapes, 2004: Radiation budget of the tropical intraseasonal oscillation. *J. Atmos. Sci.*, **61**, 2050-2062.

Lin, J. L., B. E. Mapes, M. H. Zhang and M. Newman, 2004: Stratiform precipitation, vertical heating profiles, and the Madden-Julian Oscillation. *J. Atmos. Sci.*, **61**, 296-309.

Lin, J. L., M. H. Zhang, and B. E. Mapes, 2005: Zonal momentum budget of the Madden-Julian Oscillation: The sources and strength of equivalent linear damping. *J. Atmos. Sci*., **62**, 2172-2188.

Lin, J.L., G.N. Kiladis, B.E. Mapes, K.M. Weickmann, K.R. Sperber, W.Y. Lin, M. Wheeler, S.D. Schubert, A. Del Genio, L.J. Donner, S. Emori, J.-F. Gueremy, F. Hourdin, P.J. Rasch, E. Roeckner, and J.F. Scinocca, 2006: Tropical intraseasonal variability in 14 IPCC AR4 climate models. Part I: Convective signals. *J. Climate*, **19**, 2665-2690.

Madden, R. A., and P. R. Julian, 1994: Observations of the 40-50-day tropical oscillation-A review. *Mon. Wea. Rev.*, **122**, 814-837.

Mapes, B. E., and R. A. Houze, 1995: Diabatic divergence profiles in western Pacific mesoscale convective systems. *J. Atmos. Sci.*, **52**, 1807-1828.

Mapes, B. E., and J. L. Lin, 2005: Doppler radar observations of mesoscale wind divergence in regions of tropical convection. *Mon. Wea. Rev*., in press.

Moorthi, S., and Suarez M. J., 1992: Relaxed Arakawa–Schubert: A parameterization of moist convection for general circulation models. *Mon. Wea. Rev.,* **120**, 978–1002.

Murakami, T., and T. Nakazawa, 1985: Tropical 45 day oscillation during the 1979 Northern Hemisphere summer. *J. Atmos. Sci.*, **42**, 1107-1122.

Neelin, J. D., I. M. Held, and K. H. Cook, 1987: Evaporation-Wind Feedback and Low-Frequency Variability in the Tropical Atmosphere. J. Atmos. Sci., 44, 2341-2348.

Nordeng, T.E., 1994: Extended versions of the convective parameterization scheme at ECMWF and their impact on the mean and transient activity of the model in the tropics. Technical Memorandum No. 206, European Centre for Medium-Range Weather Forecasts, Reading, United Kingdom.

Oort, A. H., and J. J. Yienger, 1996: Observed long-term variability in the Hadley circulation and its connection to ENSO. *J. Climate*, **9**, 2751-2767.

Pan, D.-M., and D. A. Randall (1998), A cumulus parameterization with a prognostic closure, *Q. J. R. Meteorol. Soc*., 124, 949-981.

Russell GL, Miller JR, Rind D, 1995. A coupled atmosphere-ocean model for transient climate change studies. Atmosphere-Ocean 33 (4), 683-730.

Schubert, S., R. Dole, H.v.d. Dool, M. Suarez, and D. Waliser, 2002: Proceedings from a workshop on "Prospects for improved forecasts of weather and short-term climate variability on subseasonal (2 week to 2 month) time scales", 16-18 April 2002, Mitchellville, MD, NASA/TM 2002-104606, vol. 23, pp. 171.

Slingo, J. M., and Coauthors, 1996: Intraseasonal oscillations in 15 atmospheric general circulation models: Results from an AMIP diagnostic subproject. *Climate Dyn.*, **12**, 325-357.

Srinivasan J., S. Gadgil, and P. J. Webster, 1993: Meridional propagation of large-scale monsoon convective zones. *Meteor. Atmos. Phys.*, **52**, 15–35.

Straub, K. H., and George N. Kiladis. 2003: Interactions between the Boreal Summer Intraseasonal Oscillation and Higher-Frequency Tropical Wave Activity. *Monthly Weather Review*, 131, 945–960.

Tiedke, M., 1989: A comprehensive mass flux scheme for cumulus parameterization in large-scale models. *Mon. Wea. Rev.,* **117**, 1779-1800.

Tokioka, T., K. Yamazaki, A. Kitoh, and T. Ose, 1988: The equatorial 30-60-day oscillation and the Arakawa-Schubert penetrative cumulus parameterization. *J. Meteor. Soc. Japan*, **66**, 883-901.

Vincent, D. G., A. Fink, J. M. Schrage, and P. Speth, 1998: High- and Low-Frequency Intraseasonal Variance of OLR on Annual and ENSO Timescales. J. Atmos. Sci., 11, 968-986.

Waliser, D., S. Schubert, A. Kumar, K. Weickmann, and R. Dole, 2003a: Proceedings from a workshop on ”Modeling, Simulation and Forecasting of Subseasonal Variability”, NASA/CP 2003-104606, vol. 25, pp. 62.

Waliser, D. E., W. Stern, S. Schubert, K. M. Lau, 2003b: Dynamic Predictability of Intraseasonal Variability Associated with the Asian Summer Monsoon, Quart. J. Royal Meteor. Soc., 129, 2897-2925.

Waliser, D. E., K. Jin, I.-S. Kang, W. F. Stern, S. D. Schubert, M.L.C Wu,K.-M. Lau, M.-I. Lee, V. Krishnamurthy, A. Kitoh, G. A. Meehl, V. Y. Galin, V. Satyan, S. K. Mandke, G. Wu, Y. Liu, and C.-K. Park, 2003c, AGCM Simulations of Intraseasonal Variability Associated with the Asian Summer Monsoon, Clim. Dyn., 21, 423-446.

Wang, B., and Linho, 2002: Rainy Season of the Asian–Pacific Summer Monsoon. J. Climate, 15, 386-398.

Wang, B., and H. L. Rui, 1990: Synoptic climatology of transient tropical intraseasonal convective anomalies: 1975-1985. *Meteor. Atmos. Phys*., **44**, 43-61.

Wang B., and X. Xie, 1996: Low frequency equatorial waves in vertically sheared zonal flow. Part I: Stable waves. *J. Atmos. Sci.*, **53**, 449–467.

Wang, W., and M.E. Schlesinger, 1999: The dependence on convective parameterization of the tropical intraseasonal oscillation simulated by the UIUC 11-layer atmospheric GCM. *J. Climate*, **12**, 1423-1457.

Webster P. J., 1983: Mechanisms of monsoon low-frequency variability: Surface hydrological effects. *J. Atmos. Sci.*, **40**, 2110–2124.

Wheeler, M., and G.N. Kiladis, 1999: Convectively Coupled Equatorial Waves: Analysis of Clouds and Temperature in the Wavenumber-Frequency Domain. *J. Atmos. Sci.,* **56**, 374-399.

Wu, M. L. C., S. Schubert, I.-S. Kang, and D. Waliser, 2002: Forced and Free Intraseasonal Variability over the South Asian Monsoon Region Simulated by 10 AGCMs. J. Climate, 15, 2862-2880.

Xie, P., and P. A. Arkin, 1997: Global precipitation: A 17-year monthly analysis based on gauge observations, satellite estimates, and numerical model outputs. *Bull. Amer. Meteor. Soc.*, **78**, 2539-2558.

Yasunari, T., 1979: Cloudiness fluctuations associated with the northern hemisphere summer monsoon. *J. Meteor. Soc. Japan*, **57**, 227-242.

Zhang, G. J. and N. A. McFarlane, 1995: Sensitivity of climate simulations to the parameterization of cumulus convection in the CCC-GCM. *Atmos.-Ocean*, **3**, 407-446.

FIGURE CAPTIONS

Figure 1. Schematic depiction of the three major components of Asian summer monsoon and its two dominant intraseasonal modes.

Figure 2. Zonal profile of boreal summer (May-October) seasonal mean precipitation averaged between (a) 5N and 25N, and (b) 25N and 40N for observation and 22 models.

Figure 3. Same as Figure 2 but for the meridional profile averaged between (a) 70E-100E, and (b) 120E-160E.

Figure 4. Seasonal variation of precipitation averaged over (a) ISM region (5N-25N, 60E-100E), (b) WNPSM region (5N-25N, 110E-170E), and (c) EASM region (25N-40N, 100E-160E).

Figure 5. Meridional profile of the total intraseasonal (2-128 day) variance of precipitation anomaly averaged between (a) 60E-100E, and (b) 120E-160E.

Figure 6. Variance of the eastward component of BSIO averaged between 5N and 25N.

Figure 7. Ratio between the variance of the eastward component of BSIO and the variance of its westward counterpart (westward wavenumbers 1-6, 24-70 day mode). The variances are averaged over an Indian Ocean box between 5N-25N and 70E-130E.

Figure 8. Lag-correlation of the 24-70 day precipitation anomaly averaged between 5N-25N with respect to itself at 15N95E. Shading denotes the regions where lag-correlation is above the 95% confidence level. The three thick lines correspond to phase speed of 3, 5, and 8 m/s, respectively.

Figure 9. Variance of the northward component of BSIO averaged between (a) 70E-100E, and (b) 120E-160E.

Figure 10. Ratio between the variance of the northward component of BSIO and the variance of its southward counterpart (southward 24-70 day mode). The variances are averaged over (a) an Indian summer monsoon box between 5N-20N and 70E-100E, and (b) an western north Pacific summer monsoon box between 5N-20N and 120E-160E.

Figure 11. Lag-correlation of the 24-70 day precipitation anomaly averaged between 70E-100E with respect to itself at 12.5N85E. Shading denotes the regions where lag-correlation is above the 95% confidence level. The three thick lines correspond to phase speed of 0.8, 1.8, and 2.8 m/s, respectively.

Figure 12. Variance of the 12-24 day mode averaged between 10N and 20N.

Figure 13. Ratio between the variance of the westward 12-24 day mode and the variance of its eastward counterpart (eastward 12-24 day mode). The variances are averaged over 10N-20N and 120E-170E.

Figure 14. Spectrum of precipitation at (a) 15N115E, and (b) 32N115E for observational data and 14 models. Frequency spectral width is 1/100 cpd.

Figure 15. Auto-correlation of precipitation at 15N115E.

Table 1 List of models that participate in this study

Modeling Groups	IPCC ID (Label in Figures)	Grid type/ Resolution/ Model top	Deep convection scheme / Modification	Downdrafts* SC/UC/Meso	Closure/ Trigger
NOAA / Geophysical Fluid Dynamics Laboratory	GFDL-CM2.0 (GFDL2.0)	Gridpoint 144*90*L24 3mb	Moorthi and Suarez (1992) / Tokioka et al. (1988)	N/N/N	CAPE/ Threshold
NOAA/ Geophysical Fluid Dynamics Laboratory	GFDL-CM2.1 (GFDL2.1)	Gridpoint 144*90*L24 3mb	Moorthi and Suarez (1992) / Tokioka et al. (1988)	N/N/N	CAPE/ Threshold
National Center for Atmospheric Research	CCSM3 (CCSM3)	Spectral T85*L26 2.2mb	Zhang and McFarlane (1995)	Y/N/N	CAPE
National Center for Atmospheric Research	PCM (PCM)	Spectral T42*L26 2.2mb	Zhang and McFarlane (1995)	Y/N/N	CAPE
NASA/ Goddard Institute for Space Studies	GISS-AOM (GISS-AOM)	Gridpoint 90*60*L12	Russell et al. (1995)	N/N/N	CAPE
NASA/ Goddard Institute for Space Studies	GISS-ER (GISS-ER)	Gridpoint 72*46*L20 0.1mb	Del Genio and Yao (1993)	Y/N/N	Cloud base buoyancy
Center for Climate System Research, National Institute for Environmental Studies, & Frontier Research Center for Global Change	MIROC3.2–hires (MIROC-hires)	Spectral T106*L56	Pan and Randall (1998) / Emori et al. (2001)	Y/N/N	CAPE/ Relative humidity
Same as above	MIROC3.2-medres (MIROC-medres)	Spectral T42*L20 30 km	Pan and Randall (1998) / Emori et al. (2001)	Y/N/N	CAPE/ Relative humidity
Meteorological Research Institute	MRI-CGCM2.3.2 (MRI)	Spectral T42*L30 0.4mb	Pan and Randall (1998)	Y/N/N	CAPE
Canadian Centre for Climate Modeling & Analysis	CGCM3.1 -T47 (CGCM)	Spectral T47*L32 1mb	Zhang & McFarlane (1995)	Y/N/N	CAPE
Max Planck Institute for Meteorology	ECHAM5/ MPI-OM (MPI)	Spectral T63*L31 10mb	Tiedtke (1989) / Nordeng (1994)	Y/N/N	CAPE/ Moisture convergence
Institute Pierre Simon Laplace	IPSL-CM4 (IPSL)	Gridpoint 96*72*L19	Emanuel (1991)	Y/Y/N	CAPE
Mateo-France / Centre National de Recherches Météorologiques	CNRM-CM3 (CNRM)	Spectral T63*L45 0.05mb	Bougeault (1985)	N/N/N	Kuo
CSIRO Atmospheric Research	CSIRO Mk3.0 (CSIRO)	Spectral T63*L18 4mb	Gregory and Rowntree (1990)	Y/N/N	Cloud base buoyancy

* For downdrafts, SC means saturated convective downdrafts, UC means unsaturated convective downdrafts, and Meso means mesoscale downdrafts.

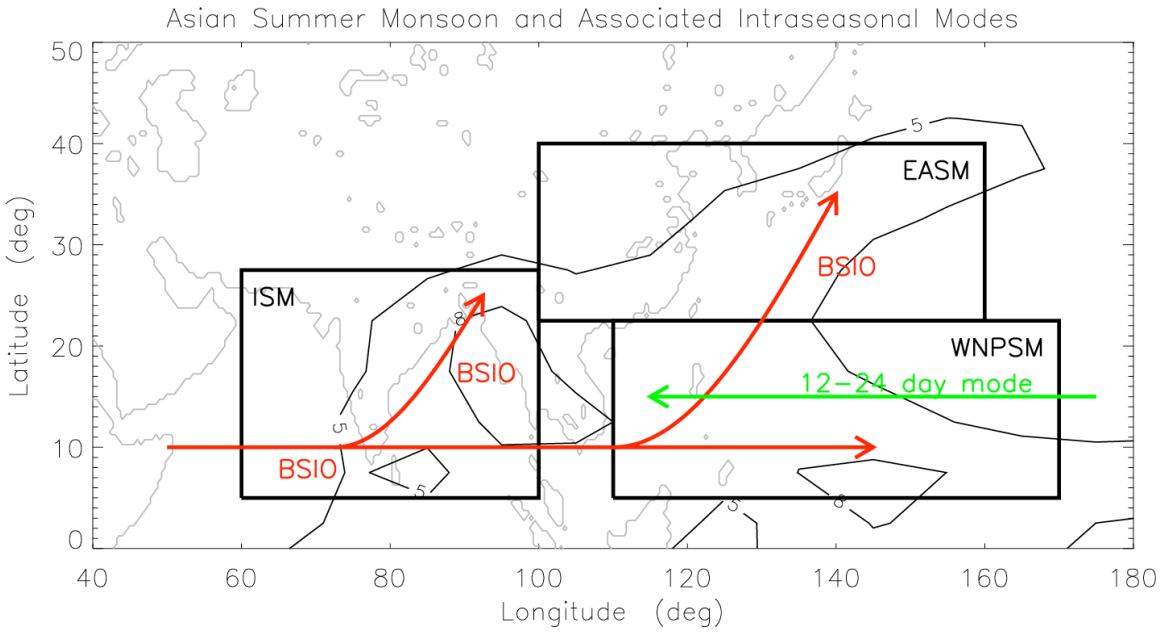

Figure 1. Schematic depiction of the three major components of Asian summer monsoon and its two dominant intraseasonal modes.

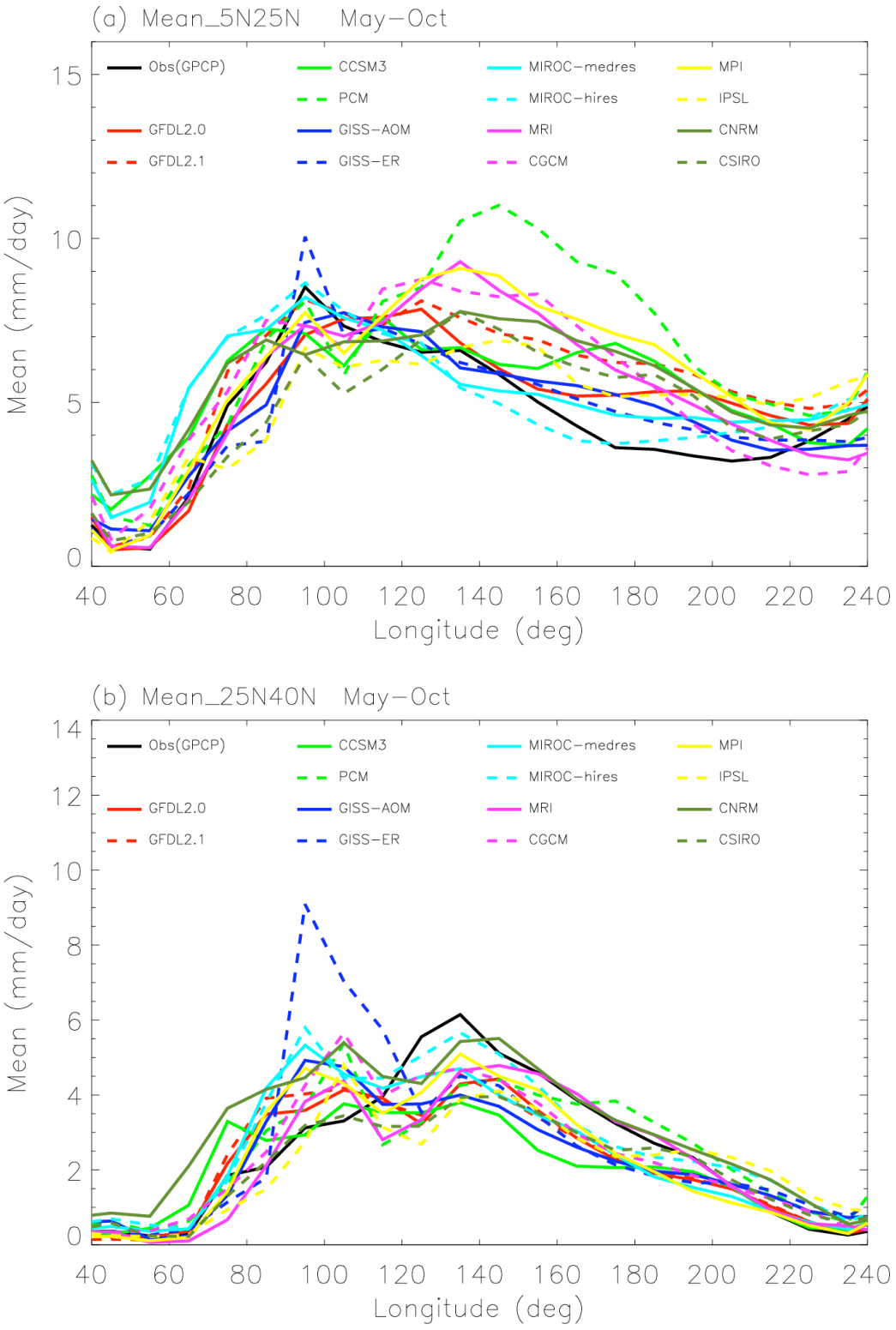

Figure 2. Zonal profile of boreal summer (May-October) seasonal mean precipitation averaged between (a) 5N and 25N, and (b) 25N and 40N for observation and 22 models.

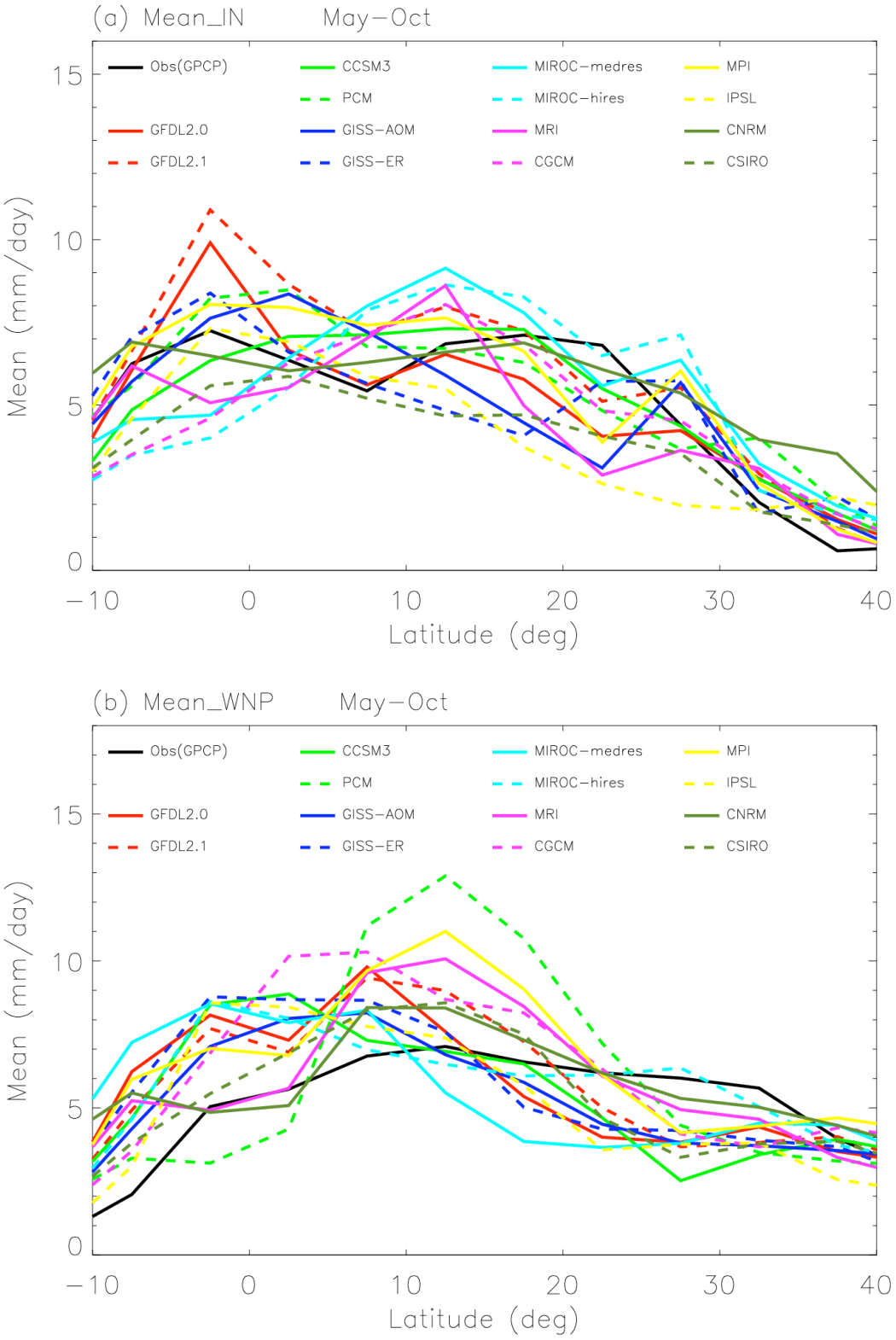

Figure 3. Same as Figure 2 but for the meridional profile averaged between (a) 70E-100E, and (b) 120E-160E.

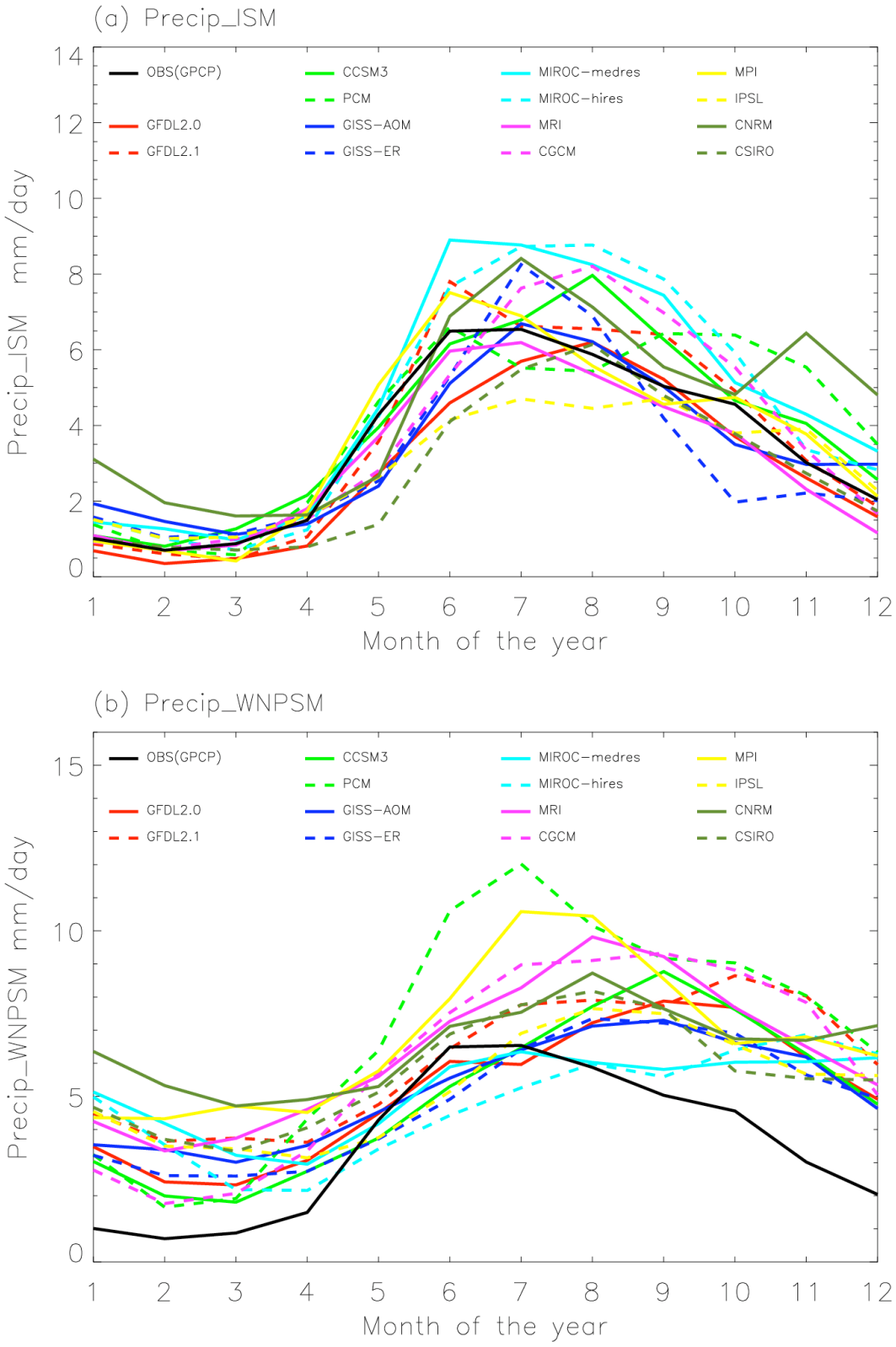

Figure 4. Seasonal variation of precipitation averaged over (a) ISM region (5N-25N, 60E-100E), (b) WNPSM region (5N-25N, 110E-170E), and (c) EASM region (25N-40N, 100E-160E).

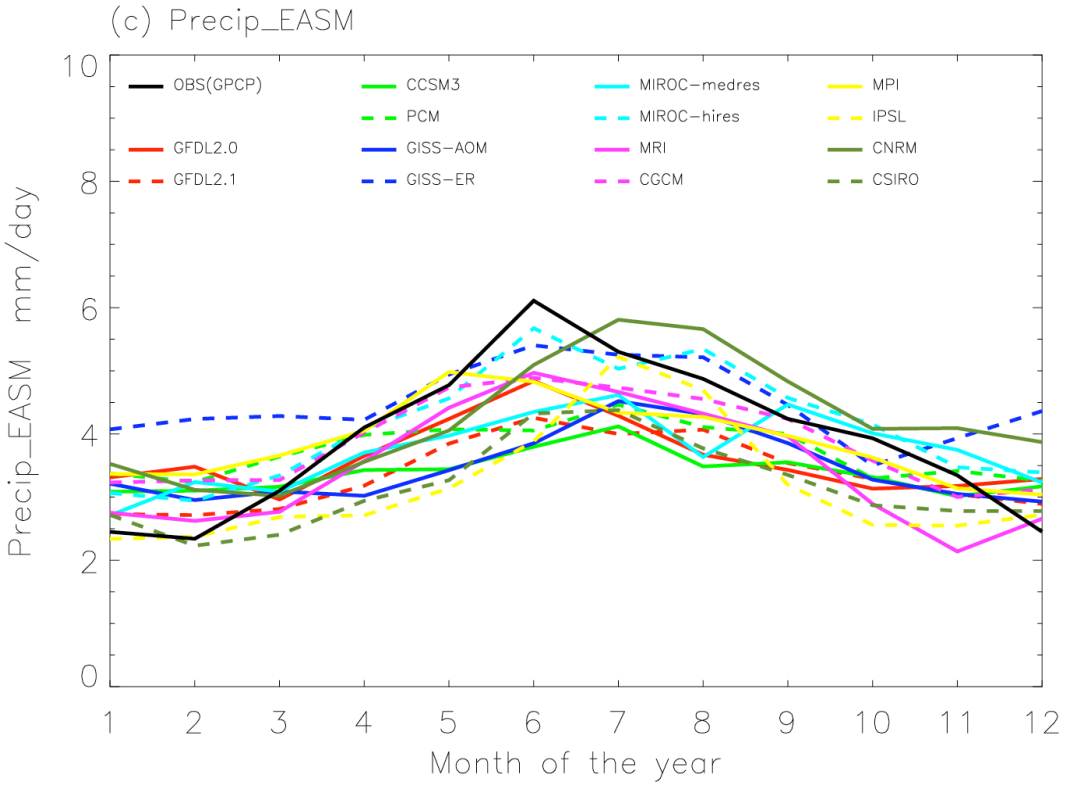

Figure 4. Continued.

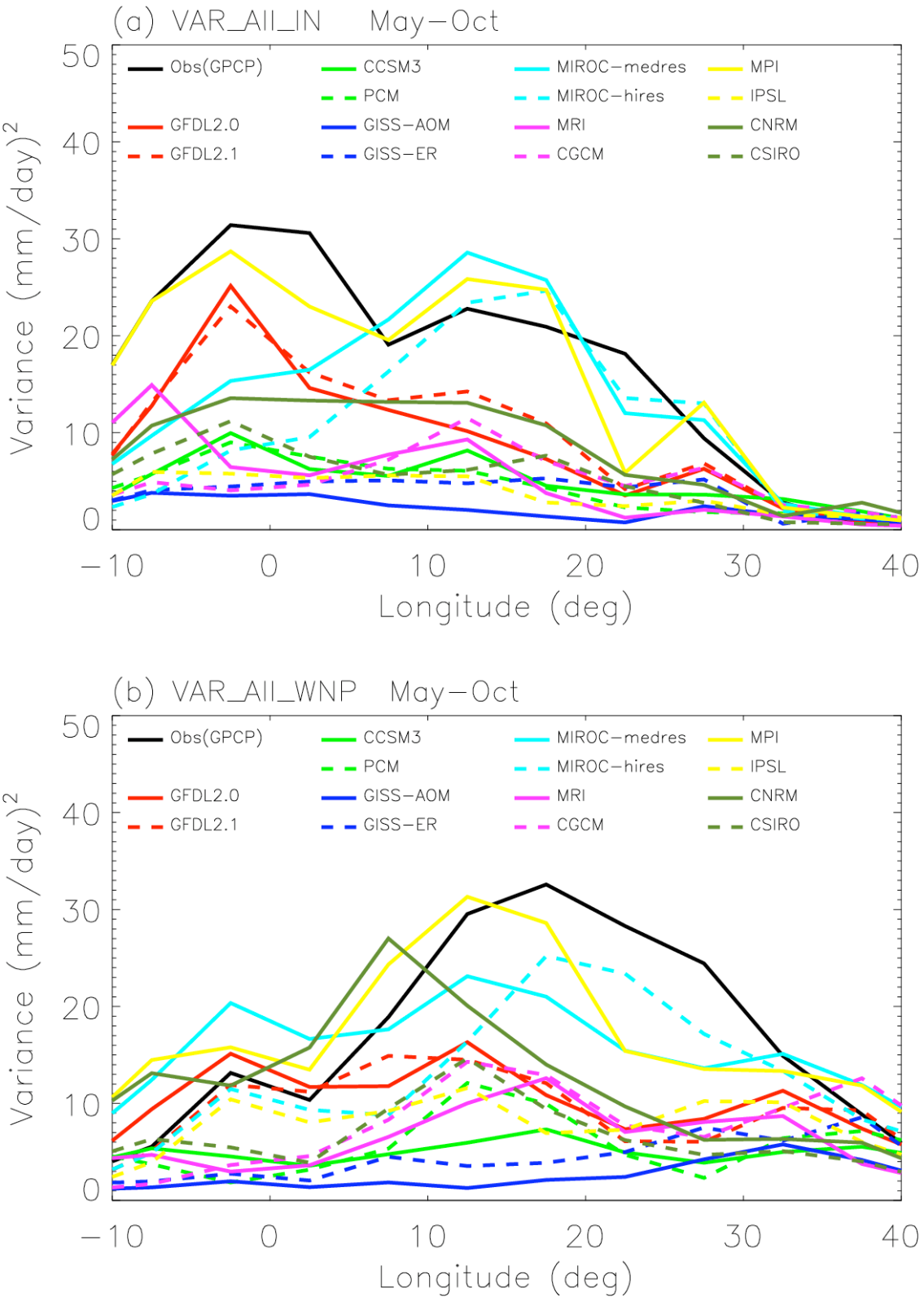

Figure 5. Meridional profile of the total intraseasonal (2-128 day) variance of precipitation anomaly averaged between (a) 60E-100E, and (b) 120E-160E.

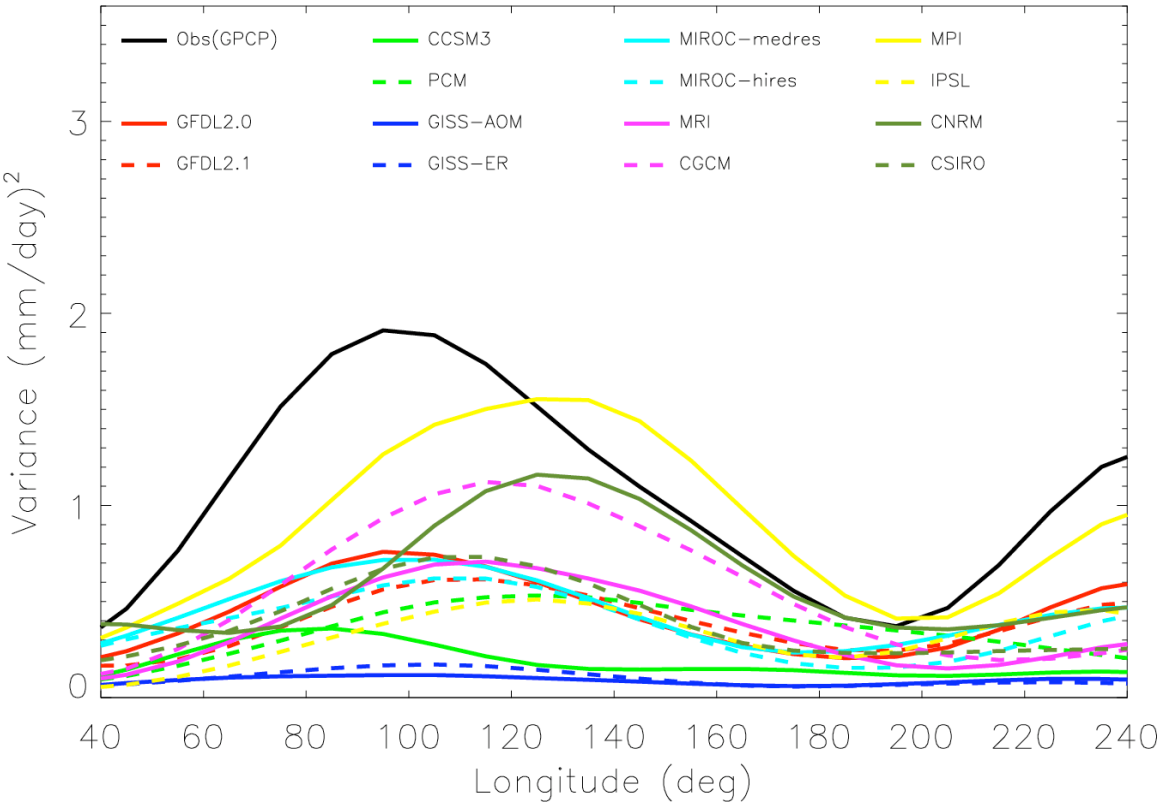

Figure 6. Variance of the eastward component of BSIO averaged between 5N and 25N.

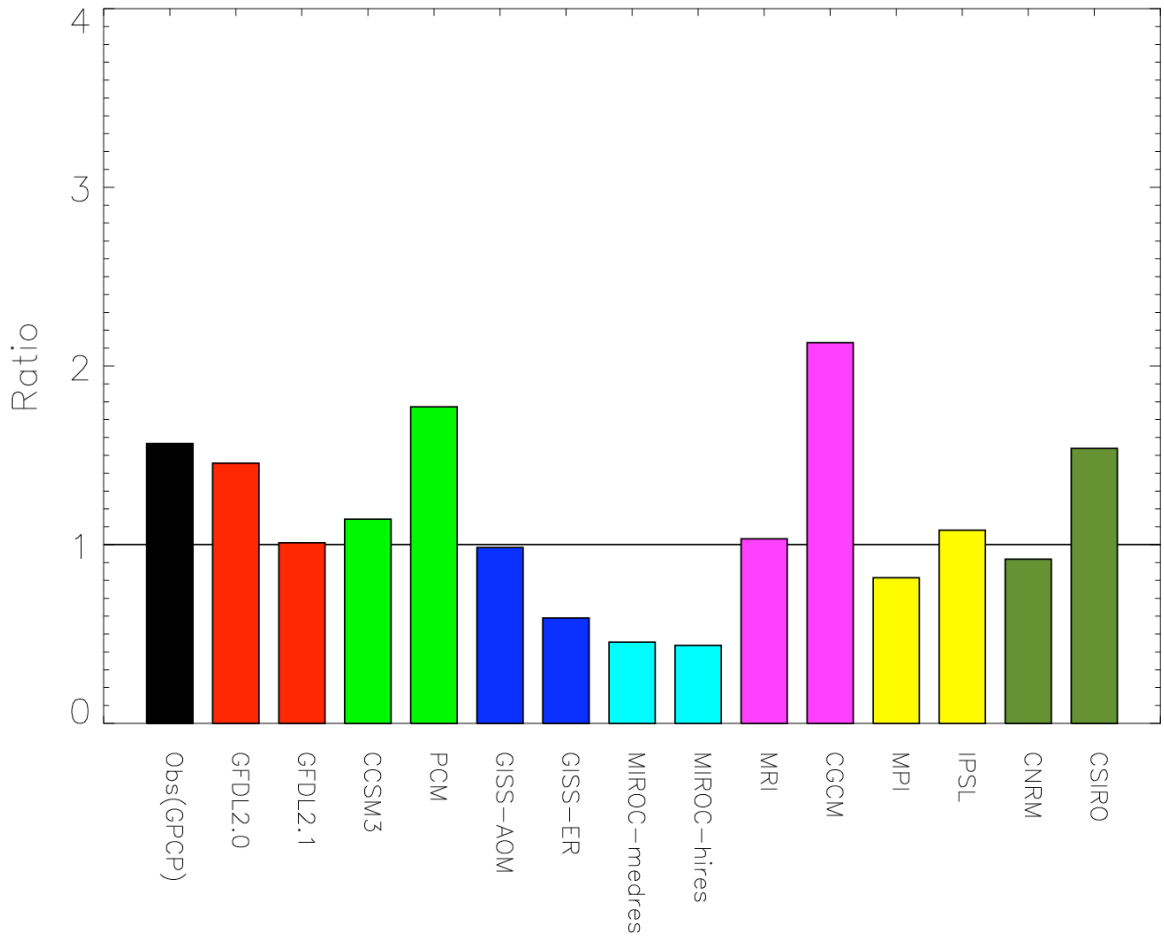

Figure 7. Ratio between the variance of the eastward component of BSIO and the variance of its westward counterpart (westward wavenumbers 1-6, 24-70 day mode). The variances are averaged over an Indian Ocean box between 5N-25N and 70E-130E.

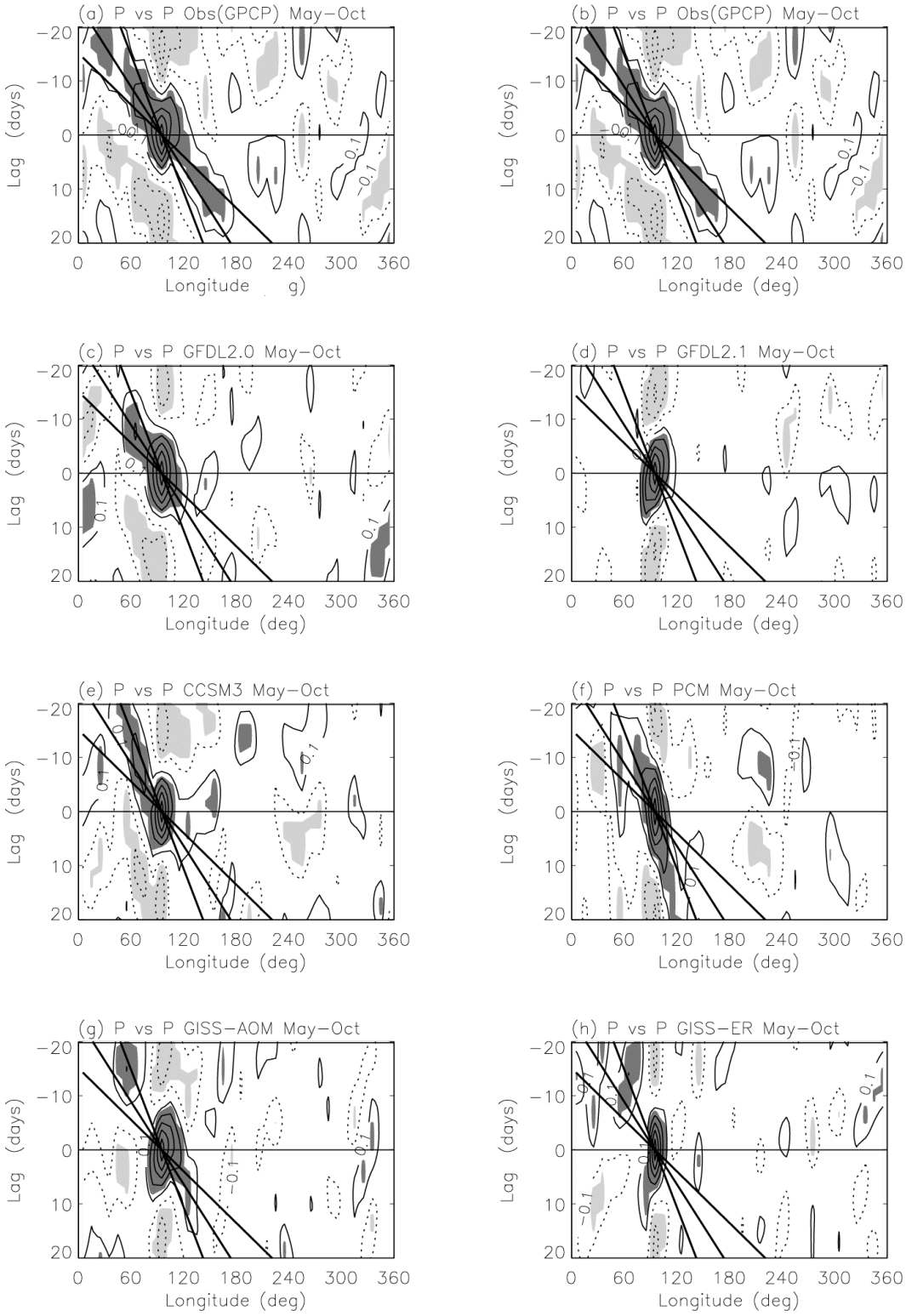

Figure 8. Lag-correlation of the 24-70 day precipitation anomaly averaged between 5N-25N with respect to itself at 15N95E. Shading denotes the regions where lag-correlation is above the 95% confidence level. The three thick lines correspond to phase speed of 3, 5, and 8 m/s, respectively.

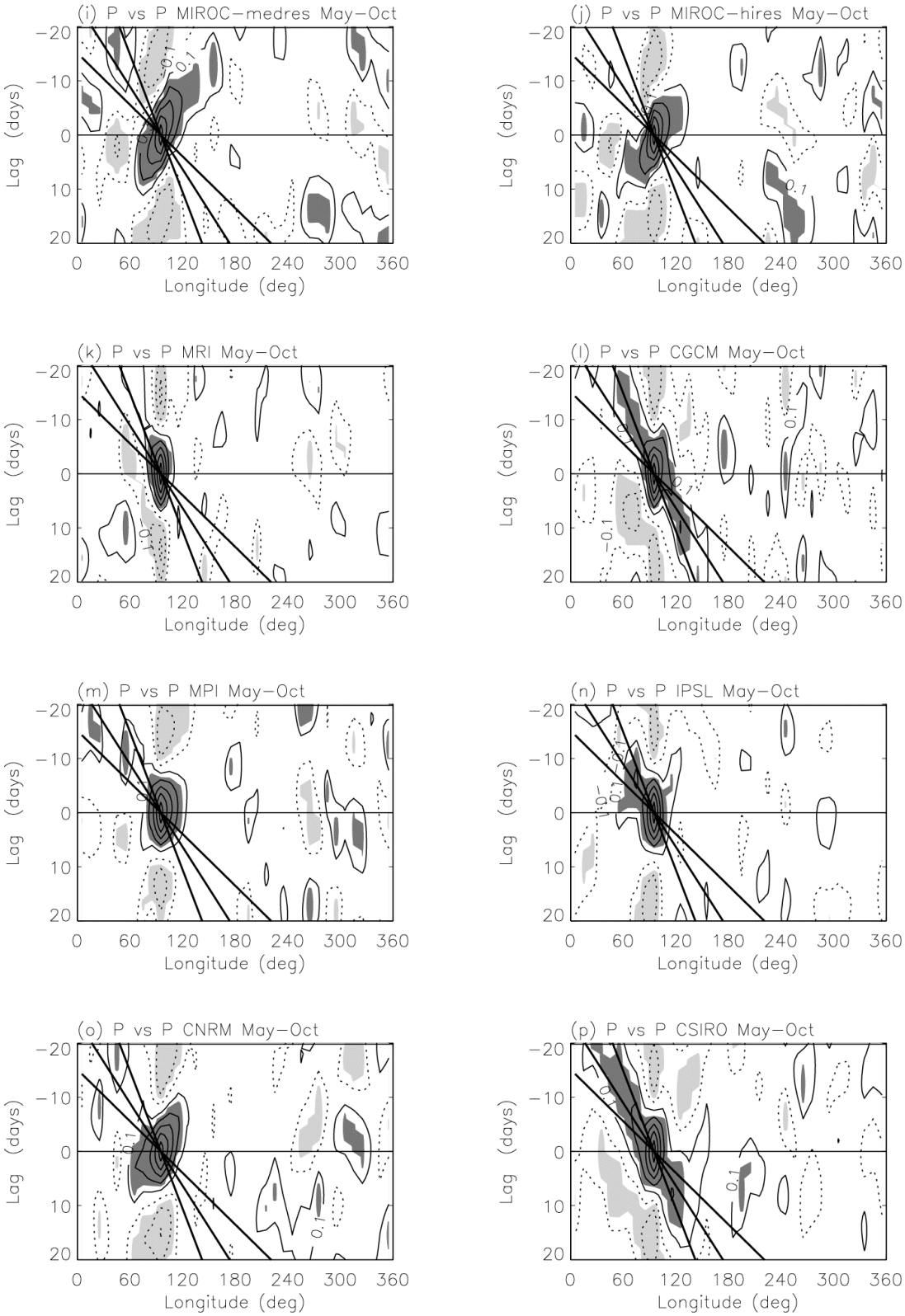

Figure 8. Continued.

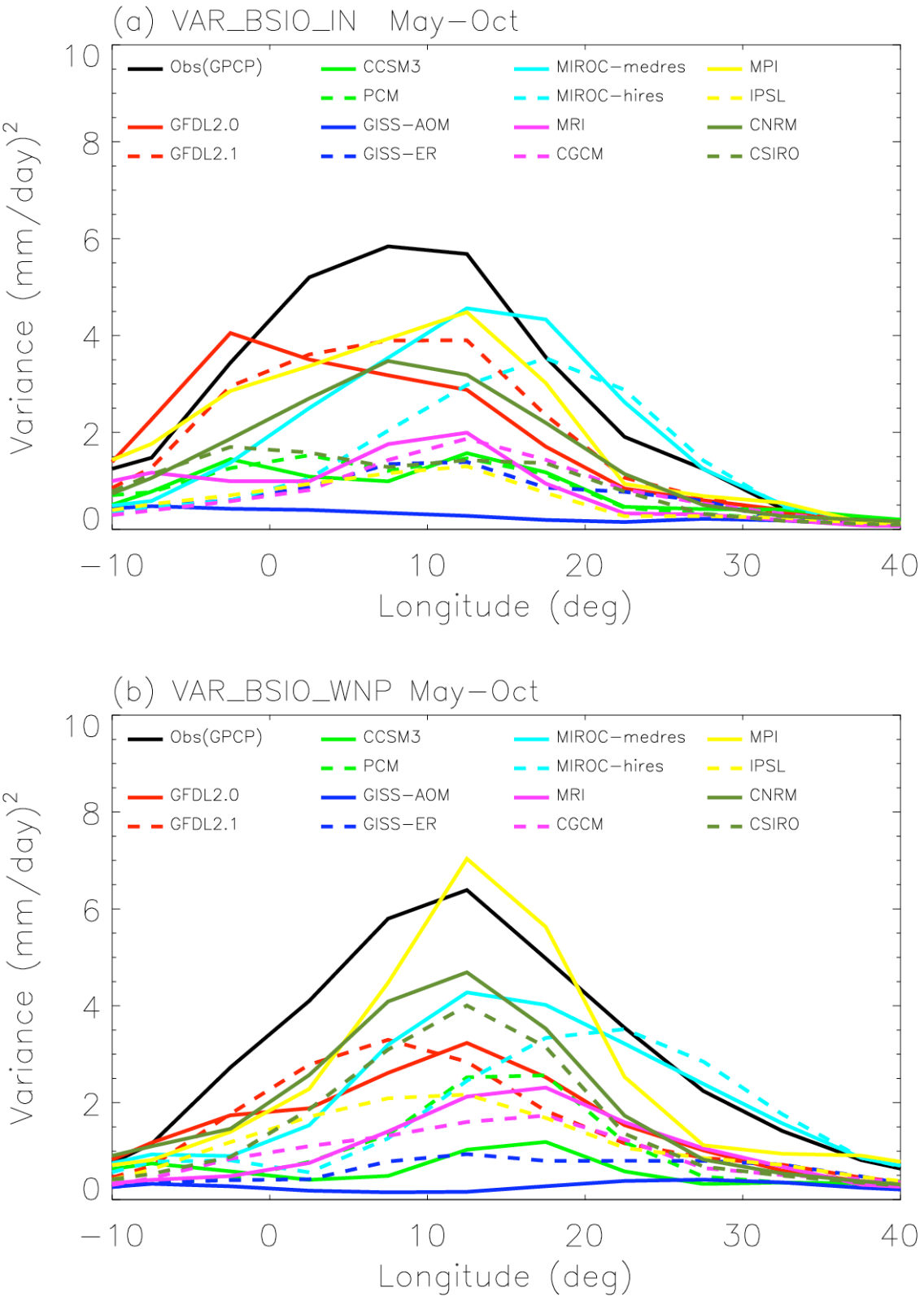

Figure 9. Variance of the northward component of BSIO averaged between (a) 70E-100E, and (b) 120E-160E.

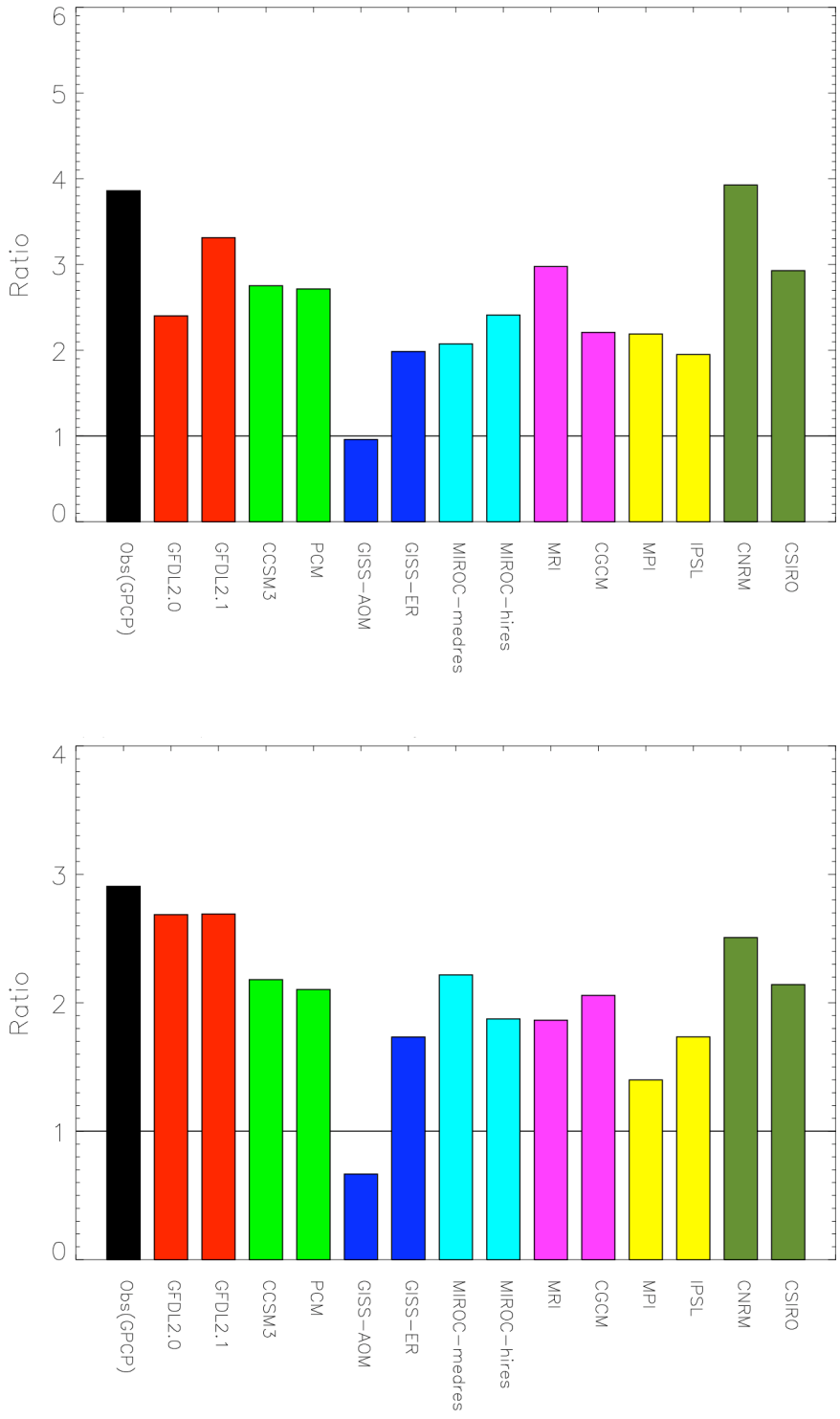

Figure 10. Ratio between the variance of the northward component of BSIO and the variance of its southward counterpart (southward 24-70 day mode). The variances are averaged over (a) an Indian summer monsoon box between 5N-20N and 70E-100E, and (b) an western north Pacific summer monsoon box between 5N-20N and 120E-160E.

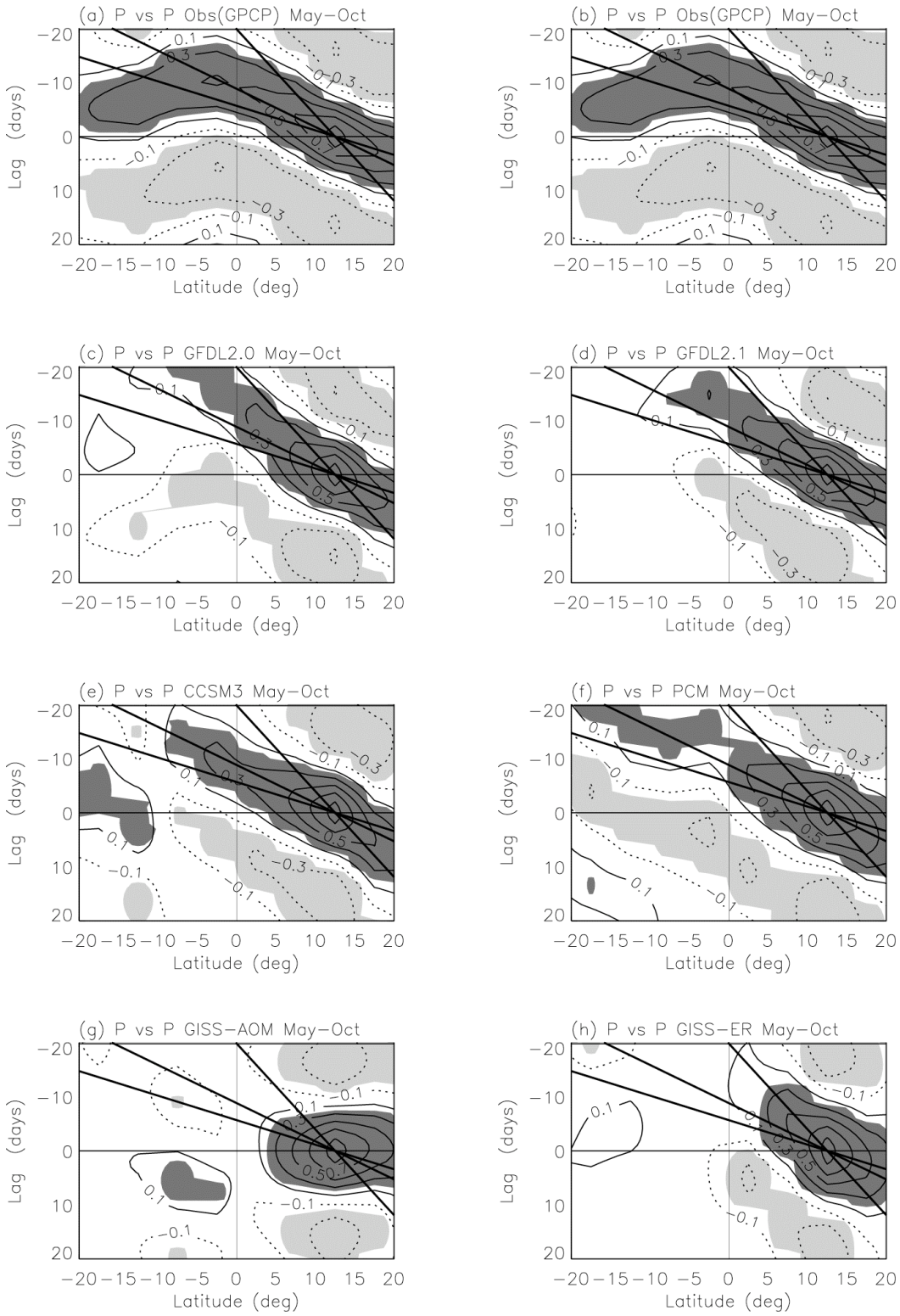

Figure 11. Lag-correlation of the 24-70 day precipitation anomaly averaged between 70E-100E with respect to itself at 12.5N85E. Shading denotes the regions where lag-correlation is above the 95% confidence level. The three thick lines correspond to phase speed of 0.8, 1.8, and 2.8 m/s, respectively.

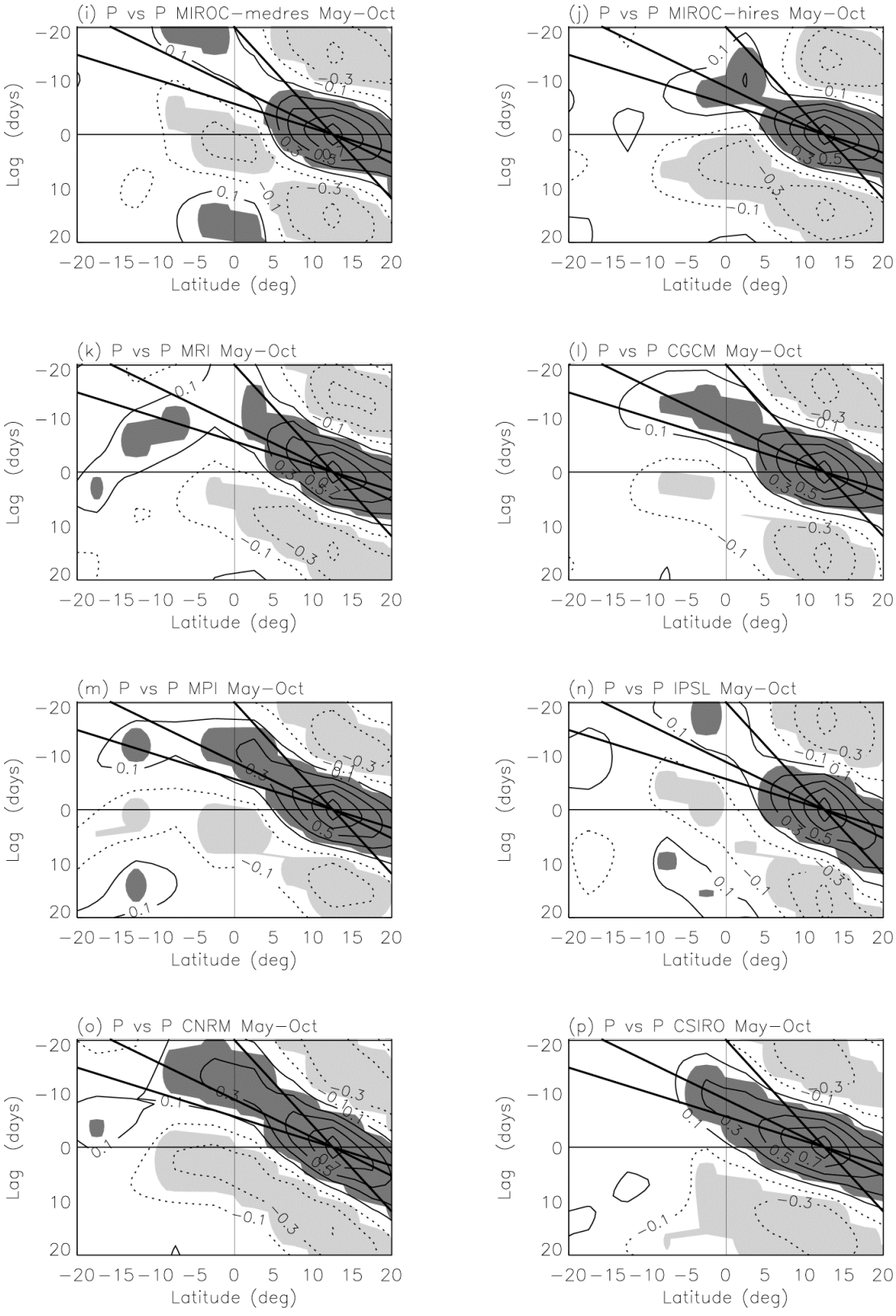

Figure 11. Continued.

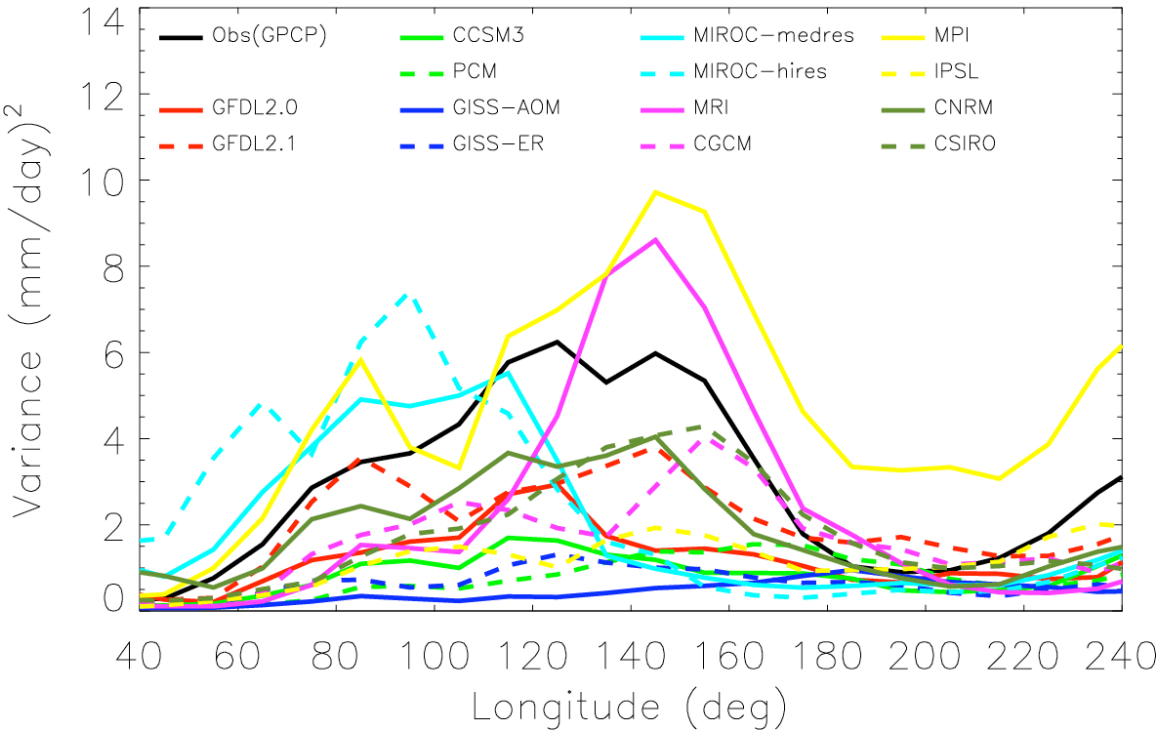

Figure 12. Variance of the 12-24 day mode averaged between 10N and 20N.

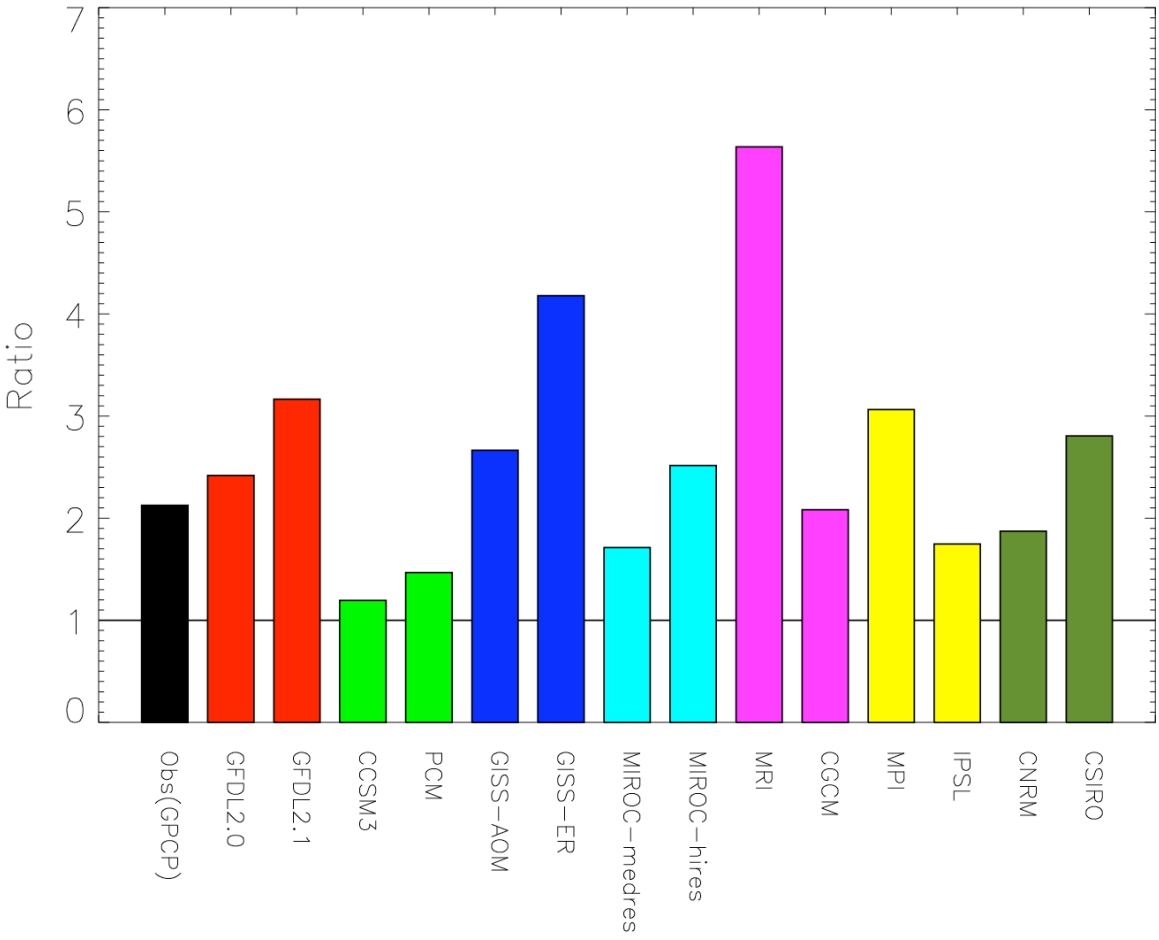

Figure 13. Ratio between the variance of the westward 12-24 day mode and the variance of its eastward counterpart (eastward 12-24 day mode). The variances are averaged over 10N-20N and 120E-170E.

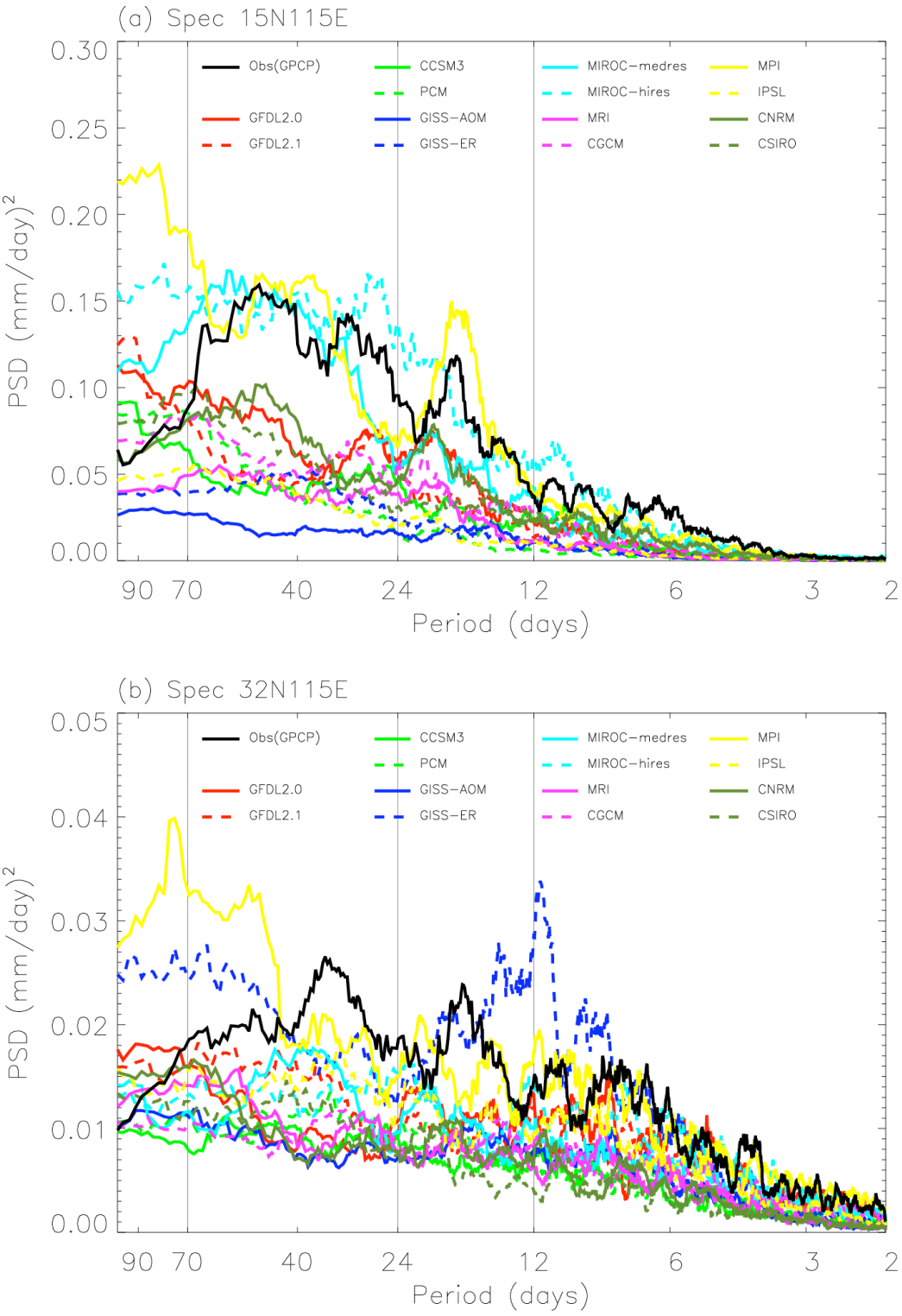

Figure 14. Spectrum of precipitation at (a) 15N115E, and (b) 32N115E for observational data and 14 models. Frequency spectral width is 1/100 cpd.

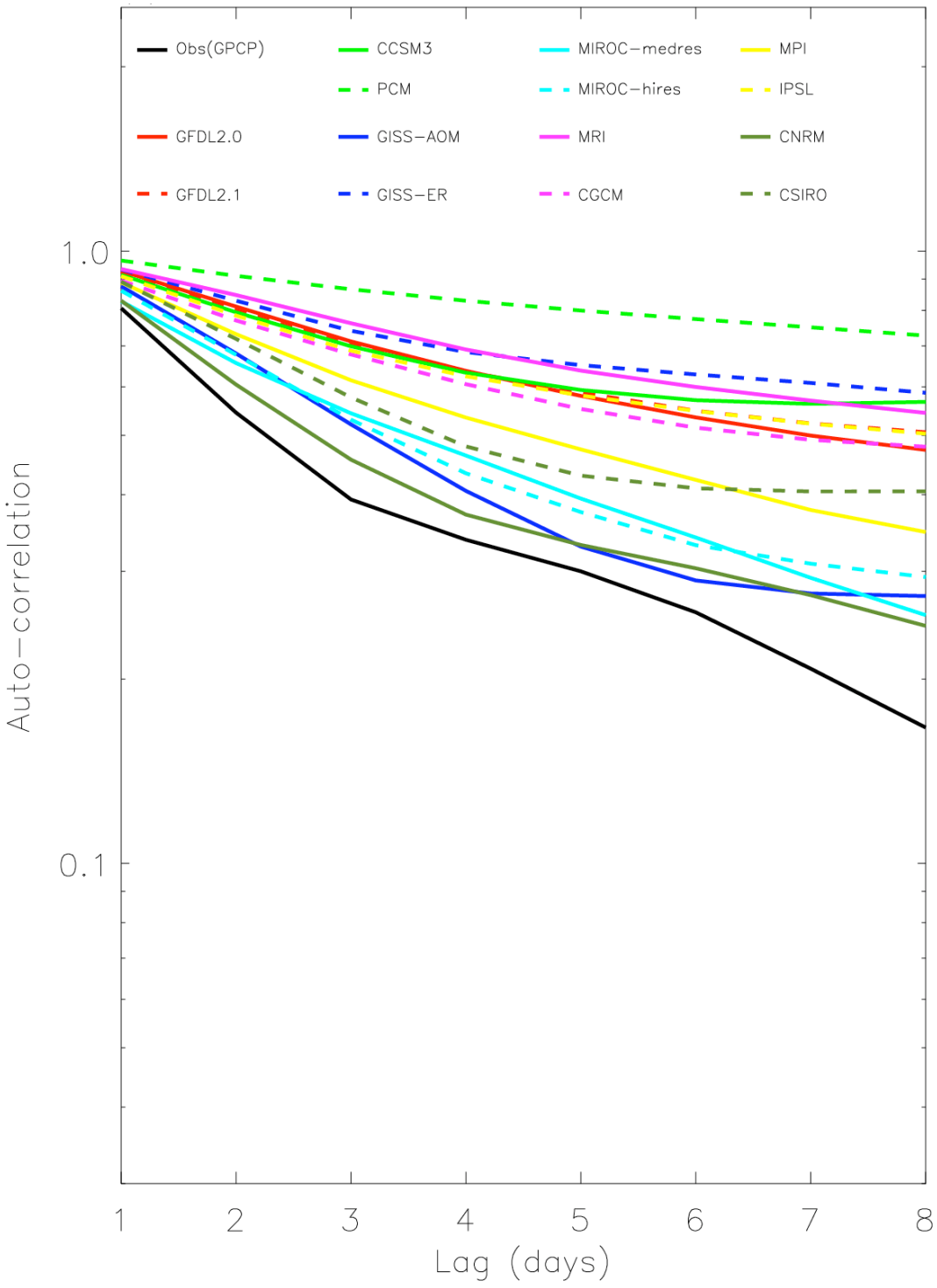

Figure 15. Auto-correlation of precipitation at 15N115E.